



HAL
open science

An integrated metabolomics and proteogenomics approach reveals molecular alterations following carbamazepine exposure in the male mussel *Mytilus galloprovincialis*

Thibaut Dumas, Frédérique Courant, Christine Almunia, Julien Boccard, David Rosain, Geoffroy Duporte, Jean Armengaud, H el ene Fenet, Elena Gomez

► To cite this version:

Thibaut Dumas, Fr ed erique Courant, Christine Almunia, Julien Boccard, David Rosain, et al.. An integrated metabolomics and proteogenomics approach reveals molecular alterations following carbamazepine exposure in the male mussel *Mytilus galloprovincialis*. *Chemosphere*, 2022, 286 (2), pp.131793. 10.1016/j.chemosphere.2021.131793 . hal-03325221

HAL Id: hal-03325221

<https://hal.science/hal-03325221v1>

Submitted on 22 Aug 2023

HAL is a multi-disciplinary open access archive for the deposit and dissemination of scientific research documents, whether they are published or not. The documents may come from teaching and research institutions in France or abroad, or from public or private research centers.

L'archive ouverte pluridisciplinaire **HAL**, est destin ee au d ep ot et  a la diffusion de documents scientifiques de niveau recherche, publi es ou non,  emanant des  tablissements d'enseignement et de recherche fran ais ou  trangers, des laboratoires publics ou priv es.



Distributed under a Creative Commons Attribution - NonCommercial 4.0 International License

1 An integrated metabolomics and proteogenomics approach reveals molecular 2 alterations following carbamazepine exposure in the male mussel *Mytilus* 3 *galloprovincialis*

4 Thibaut Dumas ¹, Frédérique Courant ^{1*}, Christine Almunia ², Julien Boccard ^{3,4}, David Rosain ¹,
5 Geoffroy Duporté ¹, Jean Armengaud ², Hélène Fenet ¹ and Elena Gomez ¹

6 ¹ HydroSciences Montpellier, IRD, CNRS, University of Montpellier, Montpellier, France;

7 ² Université Paris-Saclay, CEA, INRAE, Département Médicaments et Technologies pour la Santé (DMTS), SPI, 30200 Bagnols-
8 sur-Cèze, France;

9 ³ School of Pharmaceutical Sciences, University of Geneva, Geneva 1211, Switzerland;

10 ⁴ Institute of Pharmaceutical Sciences of Western Switzerland, University of Geneva, Geneva 1211, Switzerland

11
12 * Corresponding author at: HydroSciences Montpellier, IRD, CNRS, University of Montpellier, 15 avenue Charles Flahault,
13 34093 Montpellier, France. E-mail address: frederique.courant@umontpellier.fr

14 15 **Abstract**

16 Carbamazepine is one of the most abundant pharmaceutical active compounds detected in
17 aquatic systems. Based on laboratory exposures, carbamazepine has been proven to adversely affect
18 aquatic organisms. However, the underlying molecular events remain poorly understood. This study
19 aims to investigate the molecular mechanisms potentially associated with toxicological effects of
20 carbamazepine on the mussel *Mytilus galloprovincialis* exposed for 3 days at realistic concentrations
21 encountered in coastal environments (80 ng/L and 8 µg/L). An integrated metabolomics and
22 proteogenomics approach, including data fusion strategy, was applied to gain more insight in
23 molecular events and cellular processes triggered by carbamazepine exposure. Consistent metabolic
24 and protein signatures revealed a metabolic rewiring and cellular stress at both concentrations (e.g.
25 intensification of protein synthesis, transport and catabolism processes, disruption of lipid and amino
26 acid metabolisms). These highlighted molecular signatures point to the induction of autophagy,
27 closely related with carbamazepine mechanism of action, as well as a destabilization of the lysosomal
28 membranes and an enzymatic overactivity of the peroxisomes. Induction of programmed cell death
29 was highlighted by the modulation of apoptotic cognate proteins. The proposed integrative omics
30 data analysis was shown to be highly relevant to identify the modulations of the two molecular
31 levels, i.e. metabolites and proteins. Multi-omics approach is able to explain the resulting complex

32 biological system, and document stronger toxicological pieces of evidence on pharmaceutical active
33 compounds at environmental concentrations in sentinel organisms.

34

35 **Keywords:** Multi-omics, data fusion, pharmaceutical active compounds, mechanism of action,
36 Mediterranean mussel, marine organisms

37

38 1. Introduction

39 The antiepileptic carbamazepine (CBZ), known for its low removal in wastewater treatment
40 plants (WWTPs) ¹ and its low (bio)degradability in the environment ^{2,3}, has been proposed as a
41 possible anthropogenic marker of urban pollution in the aquatic systems ^{4,5}. CBZ is among the most
42 frequent pharmaceutical active compounds (PhACs) detected in the environment and can be a threat
43 for aquatic organisms ⁶⁻⁹. Marine ecosystems constitute the terminal receptacle of contaminated
44 continental water and are also submitted to direct discharges from WWTPs. Therefore, those
45 ecosystems are not spared by the occurrence of PhACs, including CBZ. The latter is not easily
46 adsorbed by sediments or solid particles and consequently remains mainly in the aqueous phase ^{10,11},
47 at concentrations ranging from < 1 to 1410 ng/L in marine ecosystems ^{12,13}. CBZ is thus bioavailable to
48 numerous marine organisms, especially filter feeders such as bivalve mollusks. It has already been
49 detected in tissues of marine bivalves despite its low bioaccumulation potential ¹³⁻¹⁷.

50 The exposure of marine bivalves to CBZ may lead to adverse effects. Several experimental studies
51 revealed individual and sub-individual effects at different life stages (adult, larval). The most common
52 effect reported was the induction of oxidative stress at environmental concentrations ^{18,19}. CBZ also
53 exerts various effects on marine bivalves such as cytotoxicity and immunotoxicity ²⁰⁻²⁴, genotoxicity
54 ^{22,25} and embryotoxicity ²⁶. Nevertheless, little is known about its mechanisms of action on
55 invertebrates. Some mechanisms known in humans were confirmed in marine bivalves, such as its
56 interaction with the adenylyl cyclase system leading to the reduction of intracellular cAMP levels in

57 *Mytilus galloprovincialis*²³. In addition, its potential agonist role of gamma-aminobutyric acid (GABA)
58 receptors in the clam *Ruditapes philippinarum*²¹, and its interaction with voltage-dependent Na⁺ and
59 K⁺ channels in *Scrobicularia plana*²⁷ were demonstrated. However, these different types of molecular
60 alterations are not sufficient to fully explain the adverse effects reported in the literature. Since
61 differences in CBZ pharmacokinetics and pharmacodynamics are expected between humans and
62 bivalves, it is necessary to apply non hypothesis-driven approaches to further investigate
63 mechanisms of action and toxicological effects of CBZ on marine bivalves.

64 The combination of different omics approaches (i.e., multi-omics) has been shown as a relevant
65 way to examine the complex interactions and regulation events between different biological layers
66 (e.g. DNA, RNA, proteins, metabolites)^{28,29}. Indeed, the major motivation for integrating data from
67 different levels (e.g. transcriptome, proteome, metabolome) is to improve the understanding of the
68 underlying biological system, and to gain further insight into mechanistic knowledge that is hardly
69 accessible by measuring a single level of the biological system (e.g. metabolomics alone)²⁸. According
70 to previous ecotoxicological studies, an integrated metabolomics and proteomics approach is
71 suitable to unravel mechanisms of action and toxicological effects of contaminants, without
72 preconceived assumptions³⁰⁻³². However, due to a certain degree of heterogeneity between these
73 large-scale approaches and the intrinsic complexity of the generated datasets, the integrative
74 analysis of different omics remains challenging³³. For this purpose, different fusion strategies can be
75 considered, depending on the structure and the nature of the associated data³⁴. When observations
76 constitute the common mode, i.e. the same samples are characterized by several blocks of variables
77 (e.g. metabolites and proteins), high/low/mid/ level approaches can be implemented³⁵. High-level
78 data fusion involves the individual investigation of each data block, and outputs are then collected to
79 offer a global picture of all data. One potential advantage is to provide increased prediction accuracy,
80 e.g. using a majority vote, but it does not allow links between signals from the different sources to be
81 directly considered. For that purpose, low-level data fusion constitutes an attractive alternative,
82 because the combination of data is carried out at the signal level. As relationships between multiple

83 blocks can be objectively evaluated, multiblock modelling provides a very efficient approach to this
84 aim. However, it may suffer from different sources of biological and technical noise, especially in the
85 case of multi-omics integration. In that context, mid-level strategies offer an interesting compromise
86 between these two extremes, by starting with an individual evaluation of the different blocks to
87 extract meaningful information that will be combined in a second phase. The first step of mid-level
88 data fusion can be carried out using either dimensionality reduction based on latent variable models
89 (e.g. Principal Component Analysis) or variable selection methods. The latter aims to select the most
90 informative subset of variables from each block, therefore potentially increasing prediction accuracy.
91 Another way of looking at variable selection is to remove signals that are not relevant to describe the
92 biological situation of interest. For this purpose, it is possible to implement uninformative variable
93 elimination (UVE) strategies. Processed data blocks can then be used as input of a multiblock model.
94 A mid-level data integration strategy combining Monte Carlo UVE based on partial least squares
95 regression (MCUVE-PLS)³⁶ and consensus orthogonal partial least squares-discriminant analysis
96 (consensus OPLS-DA)³⁷ was implemented in this work. By focusing on a relevant subset of variables
97 in each block, it offers the advantage of improved prediction performance compared to the whole
98 dataset, while allowing potential links between blocks to be efficiently considered. Moreover, an
99 objective evaluation of the most relevant data block(s) can be gained using multiblock modelling³⁵.

100 Hence, an integrated metabolomics and proteogenomics approach, based on mid-level data
101 fusion and multiblock modelling, can be a suitable strategy to gain understanding of biological
102 systems by reinforcing the biochemical connectivity between the two omics levels (*i.e.* proteins and
103 metabolites). Such a strategy was applied in this study to fill the information gap about the
104 mechanisms of action and potential toxicological effects of CBZ on marine bivalve mollusks. For this
105 purpose, a 3-day exposure at a low (80 ng/L) and a high (8 µg/L) dose on the Mediterranean mussel
106 *M. galloprovincialis* was conducted in controlled laboratory conditions.

107

108 2. Materials & Methods

109 2.1. Chemicals

110 Pesticide analytical-grade solvents (methanol, dichloromethane and ethanol) and LC/MS
111 grade solvents (water, acetonitrile, formic acid 99%) were obtained from Carlo Erba (Val de Reuil,
112 France). Ultrapure water was generated by a Simplicity UV system from Millipore (Bedford, MA, USA)
113 with a specific resistance of 18.2 MΩ.cm at 25°C. Analytical pure standards used for identification of
114 endogenous metabolites were purchased from the following suppliers: Sigma-Aldrich (now part of
115 Merck), Santa Cruz Biotechnology, Toronto Research Chemicals and LGC Standards. Analytical pure
116 standard used for xenobiotic quantification concern carbamazepine (CBZ, Sigma-Aldrich) and the
117 deuterated carbamazepine-d8 (CBZ-d8, Toronto Research Chemicals). All chemicals used in this study
118 were analytical grade (purity > 95 %).

119 2.2. Animals, experimental design and sample collection

120 Mussels *Mytilus galloprovincialis* were purchased from Les Compagnons de Maguelone
121 mussel culture (Villeneuve-les-Maguelone, France) in March 2019 and were brought back to the
122 laboratory in a mesh bag at room temperature (14°C) within an hour. On arrival at the laboratory,
123 mussels were immersed in seawater. Then, 90 mussels with a homogenous shell size (7.0 cm ± 0.4
124 cm) were rinsed with seawater while algae and barnacles were removed from the shell. Mussels
125 were then randomly distributed in 18 glass aquaria (n = 5 mussels per aquarium), each containing 2 L
126 of filtered seawater (provided by IFREMER, Palavas, France; filter GF/F Ø 100 µm).

127 During all the experiment (acclimatization and exposure periods), seawater was continuously
128 aerated and renewed daily, and mussels were fed once daily with the alga *Tetraselmis suecica*
129 (Greensea, Mèze, France) at constant density (10 000 cells/mL). Physicochemical parameters were
130 checked on a daily basis such as temperature (14.4 °C ± 0.5), pH (7.5 ± 0.06), oxygen (10.3 mg/L ± 0.1)
131 and salinity (36.8 ‰ ± 0.2), and were maintained constant throughout the experiment.

132 After a 7-day acclimatization period, three exposure conditions were constituted (n = 30
133 mussels *per* condition) with an environmentally relevant CBZ concentration (80 ng/L; low dose), a
134 higher CBZ concentration (8 µg/L; high dose) and a solvent control exposure (10 µl/L of methanol,
135 solvent used for the preparation of CBZ solution, corresponding to a final dilution of 0.01 ‰). Each
136 exposure solution was prepared extemporaneously every day. Aquaria seawater was spiked one hour
137 after feeding to prevent any adsorption of CBZ on the algae. Seawater (500 mL) from aquaria was
138 sampled in triplicate daily before each seawater renewal (static renewal) to quantify carbamazepine
139 concentration.

140 After three days of exposure, no dead mussels were recorded. Mussels were dissected on ice
141 to collect the digestive gland (used for both metabolomics and proteomics analysis), the gills (for
142 further analyses not in the scope of this study) and the remaining soft tissues (for CBZ
143 quantifications) in different cryotubes. In the same time, sex microscopy determination allowed the
144 identification of 17 females, 10 males and 3 undifferentiated in the solvent control exposure
145 condition, 13 females, 12 males and 5 undifferentiated in the low dose exposure condition, and 14
146 females, 12 males and 4 undifferentiated in the high dose exposure condition. The samples were
147 directly frozen in liquid nitrogen before being stored at -80°C. Metabolomics and proteomics
148 analyses were performed on the same samples in order to reinforce the biochemical connectivity
149 between the two omics levels (*i.e.* proteins and metabolites).

150 In the present study, only samples of male mussels were considered for the following
151 analysis in order to avoid any bias due to the gender confounding factor. Beside, two samples from
152 the solvent control exposure condition and two samples from the high dose exposure condition were
153 excluded from analysis due to insufficient digestive gland tissue to perform both metabolomics and
154 proteomics analysis (n = 8 males for the solvent control, n = 12 males for the low dose and n = 10
155 males for the high dose). Mussels individuals were considered independent (as the unit of
156 replication) since no clustering related to glass aquarium was observed using Principal Analysis

157 Components (PCA) or hierarchical clustering analysis for both metabolomics and proteomics analyses
158 (results not shown).

159 2.3. Extraction and analysis of carbamazepine

160 Materials and methods describing extraction and analysis of CBZ in seawater exposure and
161 mussel soft tissues were given in Supplementary Data. Briefly, extraction of CBZ in seawater
162 exposure was carried out with a solid phase extraction (SPE) method using SPE cartridges Oasis HLB
163 500 mg 6 cc (Waters, Wexford, Ireland). The extraction protocol of CBZ in mussel soft tissues was
164 based on a *QuEChERS* (Quick, Easy, Cheap, Efficient, Rugged and Safe) method adapted from
165 Martínez Bueno et al.¹⁵. The targeted analysis of CBZ was performed on a Vanquish HPLC (Thermo
166 Fisher Scientific, Bremen, Germany) coupled to a Q Exactive Orbitrap high resolution mass
167 spectrometer (Thermo Fisher Scientific, Bremen, Germany) equipped with a heated electrospray
168 ionization source (HESI).

169 2.4. Metabolomics analysis

170 2.4.1. Sample preparation

171 Digestive glands of male mussels were lyophilized and grinded until a fine powder was
172 obtained. As described in previous studies^{38,39}, the biphasic solvent system
173 methanol/dichloromethane/water (16/16/13; v/v/v) was used to extract metabolites from tissues.
174 Briefly, 30 mg of tissue (\pm 0.40 mg) were first homogenized and extracted in a glass tube with 240 μ L
175 of methanol and 75 μ L of ultrapure water and vortexed for 1 min. In the next step, 240 μ L of
176 dichloromethane and 120 μ L of ultrapure water were added before vortexing the whole 1 min. The
177 samples were left on ice for 15 min and then centrifuged at 2000 \times *g* for 15 min at 4°C. Volumes of 50
178 μ L of the supernatant (polar phase) were collected and evaporated to dryness under a nitrogen
179 stream and finally reconstituted in 200 μ L of water/acetonitrile (95/5; v/v). The extracts were filtered
180 using a 500 μ L centrifugal filter with a 10k modified polyethersulfone membrane (VWR, Fontenay-
181 sous-Bois, France), and then transferred into vials prior to liquid chromatography—high resolution
182 mass spectrometry (LC-HRMS) analysis.

183 2.4.2. *Data acquisition and quality control*

184 Non-targeted analysis was carried out using a Vanquish HPLC (ThermoFisher Scientific,
185 Bremen, Germany) coupled to a Q Exactive Orbitrap HRMS (ThermoFisher Scientific, Bremen,
186 Germany) equipped with a heated electrospray ionization source (HESI).

187 A reversed phase pentafluorophenylpropyl (PFPP) analytical column (100 × 2.1 mm; 3 μm
188 particle size; Sigma Aldrich, PA, Bellefonte, USA) was used for HPLC separation. Each sample (10 μL)
189 was loaded onto the column with a full loop injection. The mobile phase was constituted of water
190 and acetonitrile both modified with 0.1 % formic acid. The flow rate was set at 250 μL/min and the
191 gradient system was as follows (water/acetonitrile): 95/5 until 3 min, 60/40 at 8 min, 50/50 at 9 min,
192 30/70 at 13 min, 5/95 from 15 to 18 min, going back to the initial condition at 21 min (95/5) and
193 equilibrating the column until the 28th min.

194 The Q Exactive HRMS was tuned to a mass resolution of 35,000 (FWHM, m/z 200) with a
195 mass spectrum range of 50–750 m/z. Data were acquired simultaneously in both positive (ESI⁺) and
196 negative (ESI⁻) ionization modes with the following settings: spray voltage at 3.35 |kV|, sheath gas
197 flow rate of 55, aux gas flow rate at 10, S-Lens RF level of 50, capillary temperature at 300°C and
198 heater temperature at 250°C. Sample order was randomly distributed in the injection sequence to
199 avoid any bias and to reduce the influence of potential confounding factors.

200 In order to assess the analytical repeatability and sensitivity of acquisitions, a quality control
201 (QC) sample was injected at regular intervals throughout the sequence (every six samples). The QC
202 sample was prepared by pooling 40 μL of each injected sample extract. Then, the relative standard
203 deviation (RSD) for each features detected in QC samples was calculated. A controlled analytical
204 variability is set such that 70 % of features must have an RSD < 30 %⁴⁰.

205 2.4.3. *Data pre-processing*

206 The strategy for data pre-processing was already presented in Dumas et al.^{39,41}. Briefly, the
207 raw data were converted into mzXML files with MSConvert freeware (ProteoWizard 3.0)⁴². A multi-
208 step strategy was applied for processing ESI⁺ and ESI⁻ acquisitions separately using the XCMS

209 package ⁴³ in the R environment. Optimized XCMS parameters were implemented: *m/z* interval for
210 peak picking was set at 0.0025, the signal-to-noise ratio threshold was set at 10, the group
211 bandwidth was set at 8, and the minimum fraction was set at 0.5. XCMS returned results as a peak
212 table containing variable identity (i.e., *m/z* and retention time) and feature abundances (i.e. peak
213 area). After visual inspection of each extracted ion chromatogram, all features corresponding to
214 baseline drift or background noise were discarded from the peak table. In addition, the Bioconductor
215 package CAMERA ⁴⁴ was used to remove isotopes, adducts, and fragments from the peak table, thus
216 avoiding information redundancy. Based on QC sample injections, features with a RSD > 30 % were
217 excluded for statistical analysis.

218 *2.4.4. Metabolites annotation and identification*

219 The public databases Human Metabolome Database (HMDB; <http://www.hmdb.ca/>; ⁴⁵) and
220 LipidMaps (<https://lipidmaps.org/>; ⁴⁶) were used for feature annotation. A mass precision was fixed
221 at 0.002 Da. The levels of confidence for the annotation were defined according to the
222 recommendation of the Compound Identification work group of the Metabolomics Society ⁴⁷: (i) level
223 1 was characterized by unambiguous identification based on the accurate mass and retention time of
224 the corresponding analytical standard injected under the same analytical conditions (in-house
225 database), (ii) level 2 corresponded to putative annotation based upon physicochemical properties
226 and/or spectral similarity with public databases (e.g. HMDB and LipidMaps), and (iii) level 3 was
227 putatively characterized compound classes (e.g. based upon characteristic physicochemical
228 properties of a chemical class of compounds). Compound classes were attributed thanks to the
229 LipidMaps Database of Computationally-generated Bulk Lipid Species ⁴⁸.

230 *2.4.5. Differential metabolite abundance analysis*

231 Abundance of metabolites (peak area of MS spectra) was compared between the solvent
232 control condition and the CBZ treated conditions. Differential abundance was assessed with a Welch
233 *t*-test and the False Discovery Rate (FDR) was controlled using the Benjamini–Hochberg FDR

234 correction. Metabolites with an absolute significant modulation higher than 30 % (adjusted p-value <
235 0.05) were considered statistically relevant.

236

237 2.5. Proteogenomics analysis

238 2.5.1. *Protein extraction*

239 Each digestive gland, previously lyophilized, was analyzed individually by shotgun proteomics
240 in standard conditions. For this, 7 mg from each lyophilisate was mechanically homogenized by bead-
241 beating in 70 μ l of LDS sample buffer (Invitrogen, Fisher Scientific, Illkirch, France) with a Precellys
242 Evolution homogenizer (Bertin Technologies, Montigny-le-Bretonneux, France). The homogenates
243 were centrifuged at 10,000 \times g for 3 min in order to pellet cellular debris, and the resulting
244 supernatant collected to a new tube. Samples were homogenized with a mix of 0.1 mm and 0.5 mm
245 glass beads and 0.1 mm silica beads as previously recommended ⁴⁹. The homogenization was carried
246 out until the dissolution of the whole material was achieved with 5 homogenization cycles at 6800
247 rpm with a pause of 30 s between each. Then, samples were centrifuged at 16 000 \times g for 2 min.
248 Samples were then incubated for 5 min at 99 $^{\circ}$ C and briefly centrifuged. A 20 μ l aliquot of each
249 supernatant was then subjected to SDS-PAGE for a short electrophoretic migration, as described
250 previously ⁵⁰. The whole-protein content from each well was extracted as a single polyacrylamide
251 band, processed as described ⁵¹, and submitted to proteolysis with trypsin (Roche) using 0.01 %
252 ProteaseMAX surfactant (Promega).

253 2.5.2. *Liquid Chromatography - Tandem Mass Spectrometry method*

254 The peptide mixtures were analyzed in data-dependent mode with a Q Exactive HF mass
255 spectrometer (ThermoFisher Scientific) coupled with an UltiMate 3000 LC system (Dionex-LC
256 Packings). This analytical system was operated essentially as described ⁵². Peptides were resolved
257 onto a nanoscale C18 PepMapTM 100 capillary column (LC Packings) with a 90-min gradient of
258 acetonitrile, 0.1% formic acid, at a flow rate of 0.2 μ l/min. Following a Top20 method, peptides were
259 analyzed with scan cycles initiated by a full scan of peptide ions in the Orbitrap analyzer, followed by

260 high-energy collisional dissociation and MS/MS scans on the 20 most abundant precursor ions. Full
261 scan mass spectra were acquired from m/z 350 to 1800 at a resolution of 60,000. Ion selection for
262 MS/MS fragmentation and measurement was performed applying a dynamic exclusion window of
263 10 s.

264 *2.5.3. Peptide assignment and proteomics data analysis*

265 MS/MS spectra were assigned to peptide sequences by the MASCOT Daemon 2.3.2 search
266 engine (Matrix Science, London, UK) searching against the digestive gland specific RNAseq-derived
267 database obtained by *de novo* assembly with Trinity version 2.4⁵³ and followed by ORF search and
268 transcript translation with Transdecoder as described in Cogne et al.⁵⁴. The mRNA sequencing used
269 the Illumina method with paired-end 150bp sequencing strategy from which 40 millions of reads
270 were used to assemble the transcriptome. The final protein database contains 86,022 putative
271 protein sequences totaling 29,583,007 amino acids. For MS/MS spectra assignment, the parameters
272 were: full-trypsin specificity, maximum of one missed cleavage, mass tolerances of 5 ppm on the
273 parent ion and 0.02 Da on the MS/MS, carboxyamidomethylated cysteine (+57.0215) as a fixed
274 modification, and oxidized methionine (+15.9949) and deamidation of asparagine and glutamine
275 (+0.9848) as variable modifications. All peptide matches presenting a MASCOT ion score with a p-
276 value of less than 0.05, corresponding to a FDR of 1% as evaluated with the DecoyPyrat procedure⁵⁵,
277 were filtered and assigned to a protein following a parsimony rule. Functional annotation of
278 identified proteins was performed by sequence similarity search using Swissprot and NCBI nr databases
279 with the blast tool alignment DIAMOND as previously described⁵⁶. Peptide-to-spectrum matches
280 were counted for each protein leader of the protein group defined on the basis of their sequence
281 similarities.

282 *2.5.4. Differential protein abundance analysis*

283 The abundances of all MS/MS-detected proteins were based on cumulated spectral counting
284 of peptides used to identify proteins. For the differential comparison of protein abundances, spectral
285 counts were normalized as described in Liu et al.⁵⁷. Statistical evaluation of differential detection was

286 carried out using the Tfold method i.e. \log_2 (fold change), combined with a Student *t*-test for the p-
287 value calculation. The fold change was calculated according to the following ratio
288 $\frac{\text{Spectral count proteins from treated samples}}{\text{Spectral count proteins from non-treated samples (CTRL)}}$. Benjamini-Hochberg correction was applied on
289 p-values as following: $\text{adjusted } p - \text{value} = \min\left(\frac{p \times nbp}{j}, 1\right)$ using the number of proteins
290 detected with at least two different peptides for each sample (nbp), the *t*-test p-value (p) and the
291 protein rank according to the classification of increase p-value (j). A Tfold absolute value higher than
292 1 (corresponding to an up-modulation of +100 % or a down-modulation of -50 %) was considered as
293 differentially expressed between the solvent control condition and the CBZ treated conditions.

294 2.5.5. Mass spectrometry and proteomics data

295 The mass spectrometry proteomics data have been deposited to the ProteomeXchange
296 Consortium via the PRIDE⁵⁸ partner repository with the dataset identifier PXD024201 and project
297 DOI 10.6019/PXD024201. [The reviewers may access this private dataset using
298 reviewer_pxd024201@ebi.ac.uk as Username and mCyQvaJY as Password].

299 2.6. Metabolomics and proteogenomics data fusion

300 Unit variance was used as a pre-treatment to scale the variables of the different blocks. MCUVE-
301 PLS³⁶ and consensus OPLS-DA³⁷ models were computed with combinations of toolboxes and in-
302 house functions under the MATLAB[®] 8 environment (The MathWorks, Natick, USA). MCUVE-PLS was
303 carried out using the libPLS 1.98 package⁵⁹ using an ensemble of 10^4 models with a ratio of
304 calibration samples to the total samples of 0.7. A reliability index threshold of 2 was applied to
305 remove variables considered as uninformative. Then, consensus OPLS-DA was implemented using the
306 K-OPLS package⁶⁰ and leave-one-out cross-validation was performed to assess the optimal model
307 size and predictive ability. More information on MCUVE-PLS and consensus OPLS-DA are available in
308 Supplementary Data.

309 2.7. Bioinformatics analysis

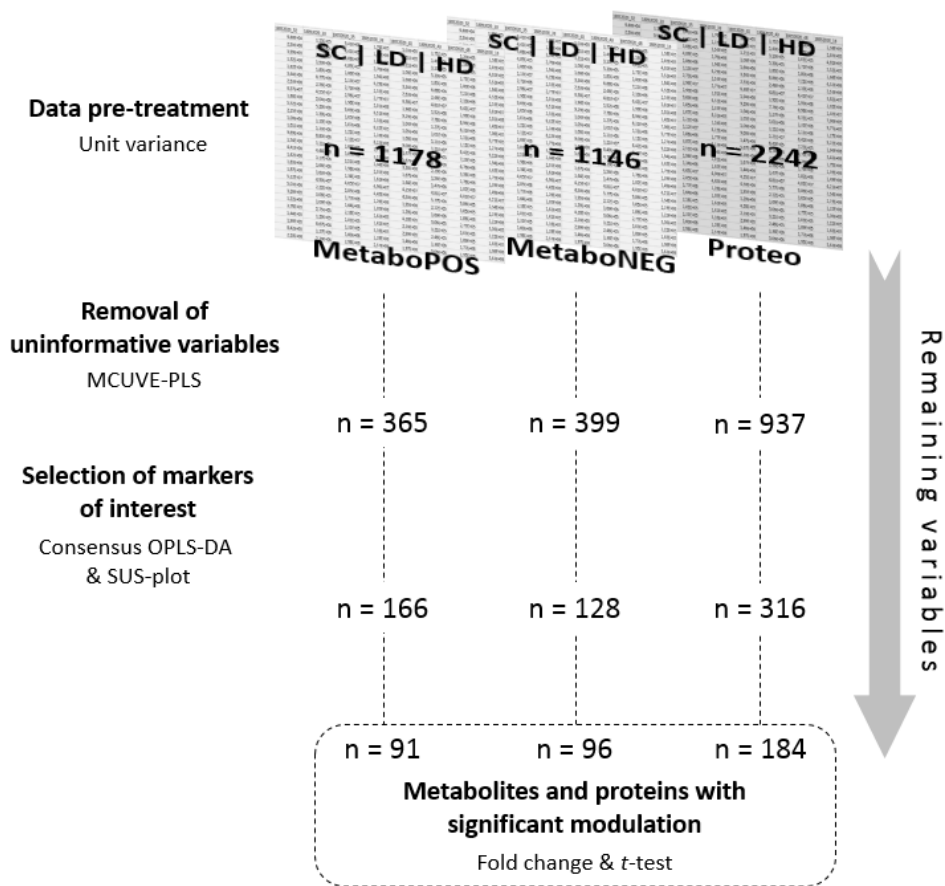
310 Bioinformatics analysis was carried out to translate metabolic or proteomic signatures, i.e. lists of
311 markers of interest, into meaningful functional information, and get deeper insights into the
312 biological events modulated by CBZ exposure. When a biological pathway is modulated in a given
313 condition, levels of the corresponding proteins and metabolites are expected to change accordingly.
314 In that context, Gene Ontology (GO) terms classification, i.e. metadata stored in databases linking
315 biological entities to a biological context, can help to highlight meaningful alterations. GO
316 classification was done for modulated proteins as previously described⁵⁶. Due to the lack of an
317 annotated genome, we used the top five homologs in the Swissprot database to associate GO terms
318 to each protein. In addition, to decipher metabolism pathways disruption by the CBZ, proteins were
319 also annotated and classified according to the KEGG pathway and KEEG BRITE databases
320 (<https://www.kegg.jp/>).

321 3. Results

322 In this study, we performed untargeted metabolomics and shotgun proteomics analyses on
323 the digestive gland of male mussels *M. galloprovincialis* exposed 3 days at two CBZ environmental
324 concentrations 80 ng/L (low dose, LD; n = 12) and 8 µg/L (high dose, HD; n = 10) and a solvent control
325 (SC; n = 8). Measured concentrations of CBZ in seawater exposure did not differ from the nominal
326 concentrations by more than 10 % (Supplementary Data). Uptake of CBZ by mussel was confirmed
327 according the CBZ concentration quantified in their soft tissues (Supplementary Data). The metabolic
328 fingerprints were constituted of 3203 signals in ESI⁻ and 5216 signals in ESI⁺, 80 % of the signals
329 having a good analytical repeatability in both ESI modes, across the QC replicates (RSD < 30 %). The
330 shotgun mass spectrometry analysis provided 864,275 Peptides Spectra Matches with a p-value
331 equal to 0.05 or lower, from the 1,891,263 spectra recorded, leading to a mean of 46 % of the
332 interpreted spectra. A number of 6,880 proteins were identified, using a parsimony method classified
333 into 5,954 groups including proteins with at least 50 % of homology.

334 3.1. Metabolomics and proteomics integrated analysis

335 Data integration was implemented using a mid-level data fusion strategy involving MCUVE-PLS
336 and consensus OPLS-DA. Figure 1 provides a comprehensive description of the statistical strategy
337 used with the remaining number of variables after each step. The metabolomic datasets acquired in
338 ESI⁺ (MetaboPOS) and ESI⁻ (MetaboNEG) as well as the proteomic dataset (Proteo) were defined as
339 three separate data blocks, accounting for 1178, 1146 and 2422 variables, respectively. These
340 variables were considered as acceptable according to analytical criteria (e.g. QC RSD < 30 %,
341 exclusion of isotopes, exclusion of signals with a retention time out of the analytical acquisition
342 time). First, the three data blocks were processed individually and MCUVE-PLS was carried out to
343 remove uninformative variables. A reliability index cut-off of 2 was found appropriate to remove
344 unwanted signals, while preserving biological information. Subsets of 365 variables, representing 31
345 % of the total from the corresponding block, 399 (35 %) and 937 (39 %) variables were obtained for
346 the MetaboNEG, MetaboPOS and Proteo blocks, respectively.



347

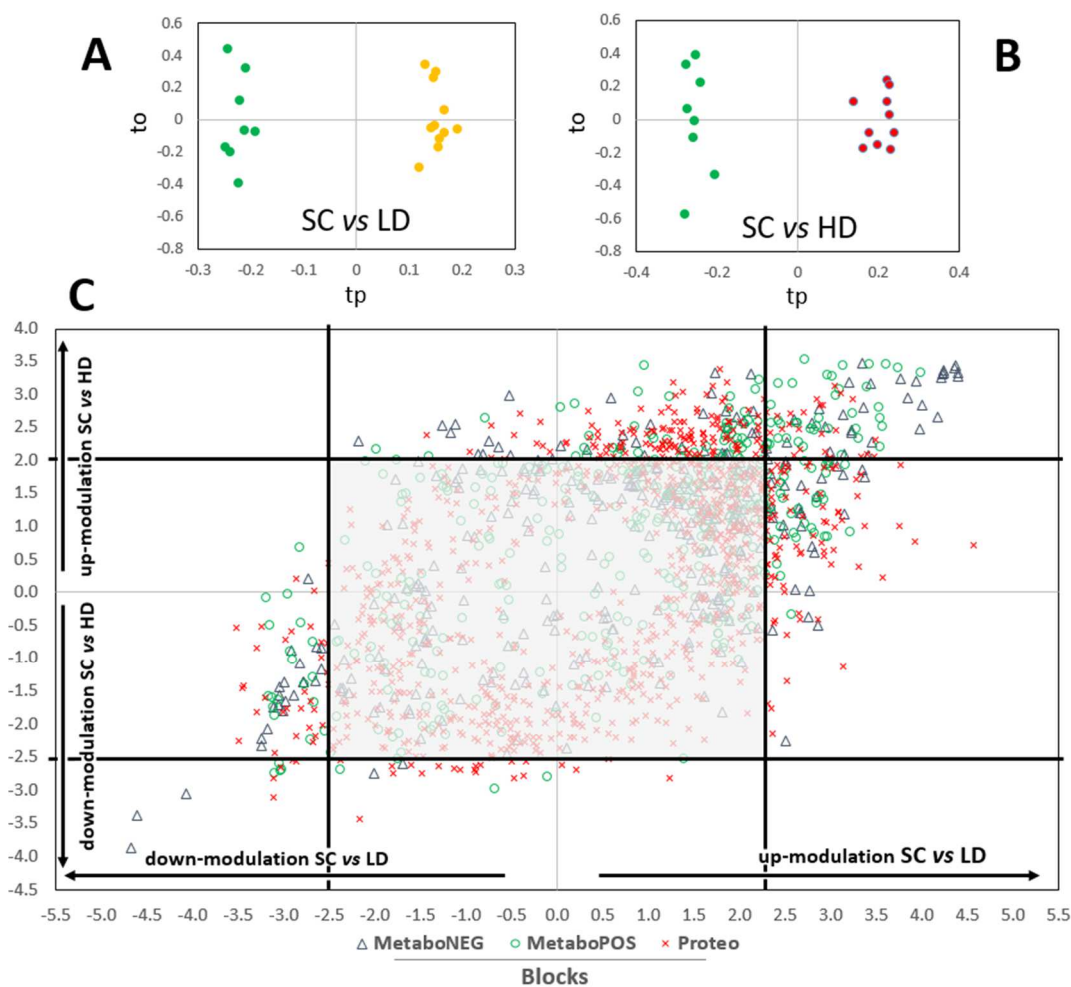
348 **Figure 1:** Strategy for selection of statistically relevant proteins and metabolites, and the remaining variables after each
 349 step for the respective blocks MetaboPOS (metabolomics dataset acquired in ESI+), MetaboNEG (metabolomics dataset
 350 acquired in ESI-) and Proteo (proteomics dataset).

351 Two consensus OPLS-DA models comparing the solvent control (SC) to each exposure condition
 352 separately, i.e. low dose 80 ng/L (SCvsLD) and high dose 8 µg/L (SCvsHD), were then evaluated. Both
 353 models were found optimal with two components (one predictive and one orthogonal) using leave-
 354 one-out cross-validation. The SCvsLD model was characterized by R2Y=0.990 and Q2Y=0.851 (Figure
 355 2A), while the SCvsHD was associated with R2Y=0.985 and Q2Y=0.811 (Figure 2B), indicating that
 356 each model explained more than 98 % of the data and has a predictive performance higher than 80
 357 %.

358 A Shared and Unique Structure (SUS) plot was then used to distinguish signals with common
 359 patterns of variations associated with both doses, from specific modulations related to a given
 360 exposure condition (Figure 2C). The coordinates of the signals on the SUS-plot were defined
 361 according to their loading provided by each consensus OPLS-DA model (abscissa axis: loading from
 362 the SCvsLD model; ordinate axis: loading from the SCvsHD model). Interestingly, the distribution of

363 the data points suggested an overall common modulation resulting from the two doses. Moreover,
 364 the lower density at the center of the plot was the consequence of the elimination of variables
 365 considered as non-informative by MCUVE-PLS. Thresholds were set to select the extreme data points
 366 of the SUS-plot associated with markers of interest. These variables were expected to be the most
 367 informative according to the models to explain the effects of CBZ at the low and high dose of
 368 exposure on the modulation of proteins and metabolites.

369 Hence, the selected signals considered as relevant included subsets of 128, 166 and 316 signals
 370 from the blocks MetaboNEG, MetaboPOS and Proteo, respectively. Among these selected signals, 45
 371 were annotated from the block MetaboNEG, 37 from the MetaboPOS and 316 from the Proteo. The
 372 annotations are provided in Tables S1 and S2 for metabolites and proteins, respectively.



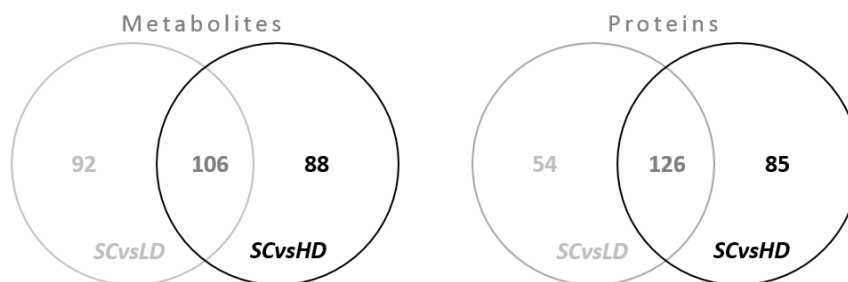
373
 374 **Figure 2:** Score plots of the two consensus OPLS models with one orthogonal component (to) and one predictive
 375 component (tp): (A) solvent control exposure versus low dose exposure (SCvsLD) and (B) solvent control versus high dose
 376 (SCvsHD). (C) Shared and Unique Structure (SUS) plot integrating both comparisons SCvsLD and SCvsHD with common and
 377 specific modulations. Variables with a blue triangle belong to the MetaboNEG block (metabolomics dataset acquired in ESI-

378), those with a green circle to the MetaboPOS block (metabolomics dataset acquired in ESI-) and those with a red cross to
379 the Proteo block (proteomics dataset). The thresholds are represented with black lines and variables with a variation
380 considered less relevant are shaded.

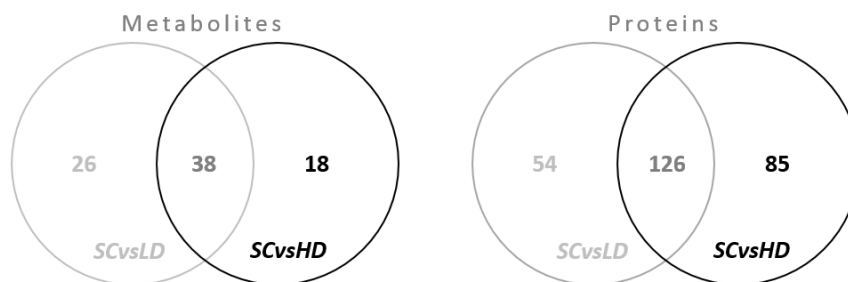
381 In order to highlight the significantly modulated proteins and metabolites, their modulation
382 amplitude and p-value for both comparisons SCvsLD and SCvsHD were indicated in Tables S1 and S2.
383 As expected, all the selected signals had not necessarily a significant modulation amplitude,
384 especially for proteins. As no pre-selections of the metabolites and proteins was done on the basis of
385 the modulation of their abundance, the selection of proteins and metabolites from the SUS-plot was
386 not only based on a significant modulation, but mainly depended on correlation patterns between
387 the variables. Compounds with a non-significant modulation amplitude, but localized at the extremes
388 of the SUS-plot data points, may have a high correlation with other compounds, and the latter could
389 have an important biological meaning. Therefore, selected (and annotated) signals with a modulation
390 trend considered as relevant on the SUS-plot were selected for subsequent bioinformatics analyses.

391 Venn diagrams were built to highlight the number of metabolites or proteins with a common
392 or specific modulation between the exposure conditions (Figure 3). Among the selected metabolites
393 or proteins, less than half had a common modulation between the low and high dose of exposure.
394 Hence, CBZ seemed to have partially similar effect at both doses but also some dose specificities.
395 When looking at annotated signals, the common and specific patterns of modulation between the
396 two doses were globally conserved, although less than one third of the metabolites could be
397 annotated (Figure 3).

Selected



Annotated

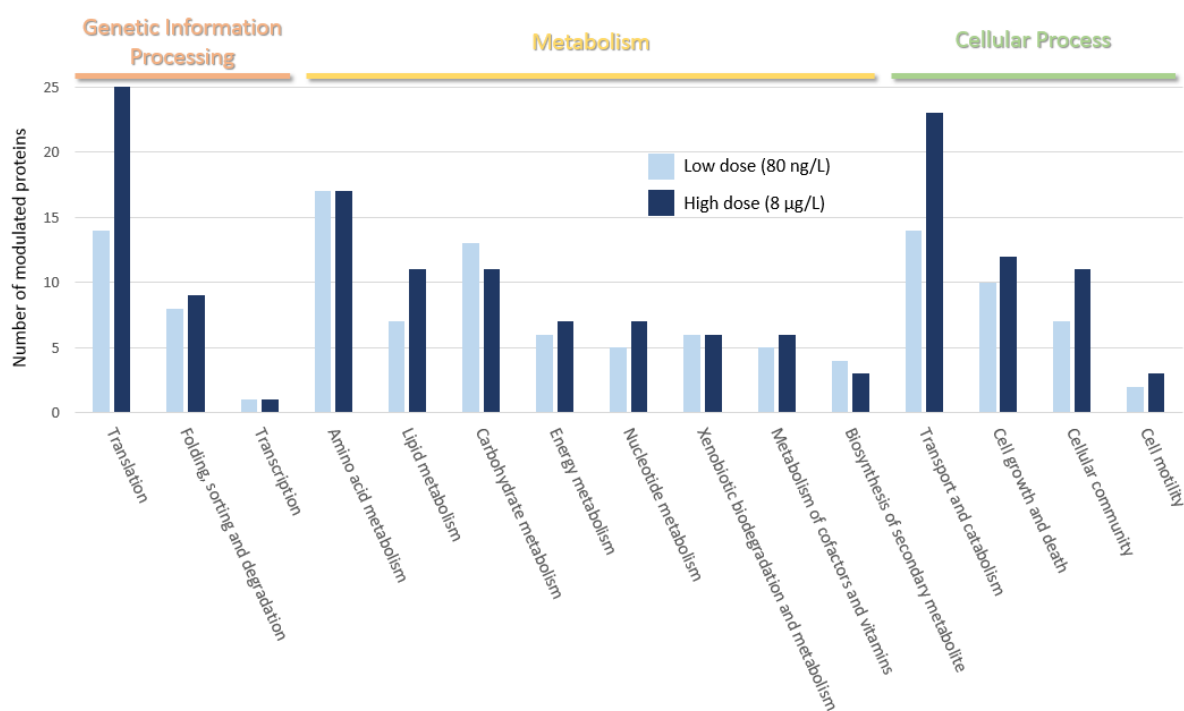


398
399 **Figure 3:** Venn diagrams highlighting specific and common variable modulations (metabolites and proteins) between both
400 comparisons solvent control exposure versus low dose exposure (SCvsLD), and solvent control versus high dose (SCvsHD).
401 Results are given for the selected signals according to the SUS-plot and then for annotated ones.

402 Bioinformatics tools were used to highlight biological processes and functions potentially
403 altered by CBZ exposure from the selected subsets of proteins and metabolites. Finally, both proteins
404 and metabolites were employed for a global analysis of metabolic pathways, in order to describe the
405 relationships between both omics levels.

406 3.2. CBZ effects on proteome

407 Modulated proteins were queried against KEGG and assigned to pathways, themselves
408 classified in three categories: genetic information processing, metabolism and cellular process
409 (Figure 4). Not all the proteins queried against the KEGG database could be assigned to a KEGG ID,
410 and the number of modulated proteins successfully associated to KEGG pathways was 97 for the low
411 dose (73 % of the selected proteins) and 127 for the high dose (74 % of the selected proteins).



412 **Figure 4:** KEGG pathways in which the modulated proteins are involved at the low and high dose of carbamazepine.
 413

414 The classification of proteins according to KEGG databases (Figure 4) highlighted cellular and
 415 metabolic processes largely impacted by proteins modulated at low or high doses. These processes
 416 were mainly related to translation process (twice the amount of protein modulated at the high dose),
 417 transport and catabolism (more pronounced at the high dose), metabolisms of amino acids and
 418 carbohydrates (equally between the two doses), degradation of lipids (more pronounced at the high
 419 dose) and cell growth and death (equally between the two doses).

420 An intensification of the translation process can be highlighted through the increasing
 421 number of modulated ribosomal proteins at the low dose (6 ribosomal proteins up-modulated and 6
 422 down-modulated) and, to a greater extent at the high dose (19 ribosomal proteins mainly up-
 423 modulated) (Table S2). Increased numbers of ribosomal proteins lead to increases in the amount of
 424 RNA transcription and protein synthesis. The steps following translation, involving the folding and
 425 maturation of newly synthesized proteins, the sorting and the degradation of misfolded proteins,
 426 were also disturbed through the modulation of proteins within the endoplasmic reticulum (ER) at
 427 both doses (Figure S1). For example, the following proteins from ER were significantly up-modulated
 428 at the low and high dose, respectively: mannosyl-oligosaccharide 1,2- α -mannosidase IA (ERManI)

429 (+1340 % and +900 %), dolichyl-diphosphooligosaccharide--protein glycosyltransferase subunit
430 STT3B-like (STT3) (+140 % and + 160 %), protein ERGIC-53 (+120 % and +120 %), while UDP-
431 glucose:glycoprotein glycosyltransferase 1-like isoform X1 (HUGT) was significantly up-modulated
432 only at the high dose (+70 %). Through an intensification of translation and ER activity, CBZ exposure
433 induces protein synthesis and degradation of misfolded proteins. Accumulation of misfolded proteins
434 can cause stress of ER. Significant up-modulations of two markers of ER stress were observed: bax
435 inhibitor-1 protein (+1245 % at the low dose and +885 % at the high dose) and sarco/endoplasmic
436 reticulum calcium ATPase (+200 % at the low dose and +160 % at the high dose).

437 Transport and catabolism processes appeared to intensify at the low dose and, to a greater
438 extent, at the high dose (Figure 4). As described in Table S3, several proteins, mainly up-modulated,
439 were involved in the internalization of compounds into the cell by endocytosis/phagocytosis. This
440 also includes the degradation of compounds and cellular components mainly via the autophagic-
441 lysosomal system, but also by phagolysosomes (fusion of lysosome with phagosome), and
442 peroxisomes. Regarding the high number of down- and up-modulated proteins involved in the
443 autophagic-lysosomal system (Table S3), CBZ triggered certain mechanisms inducing autophagy at
444 the both doses. The most modulated protein was Bax inhibitor-1 protein, involved in the regulation
445 of autophagy after ER stress. Another protein that may be related to autophagy induction is inositol
446 monophosphatase 1, significantly up-modulated at the low and high doses (+328 % and +245 %,
447 respectively).

448 Cell growth and death was the second most enriched cellular process at both doses
449 (Figure 4). More specifically, modulated proteins belonged mainly to the cell death process that
450 includes apoptotic processes. Induction of apoptosis was supported by several proteins that were
451 significantly, or slightly, modulated at the high dose, such as TNF ligand-like 1 (+160 %; p-value =
452 0.042), TNF ligand superfamily member 10 (+40 %; p-value = 0.068), caspase 2 (-30 %; p-value =
453 0.067), cathepsin B (+80 %; p-value = 0.015) and mitogen-activated protein kinase kinase 1 (+470 %;
454 p-value = 0.0015). At the low dose, the modulation of the quinone oxidoreductase PIG3-like isoform

455 X2 (-60 %; p-value = 0.016) from the p53 signaling pathway could be involved in the induction of
456 apoptosis by generating oxidative stress. At the same dose, we also observed a tendency towards
457 down-modulation of caspase 2 (-30 %; p-value = 0.059) and up-modulation of cathepsin B (+50 %;
458 0.081) as well as significant up-modulation of mitogen-activated protein kinase kinase (+400 %; p-
459 value = 0.024), supporting the induction of programmed cell death even at an environmental
460 concentration of CBZ.

461 Regarding metabolic pathways, most of the modulated proteins matched with the amino
462 acid metabolism (17 proteins) and carbohydrate metabolism (13 proteins), while no marked
463 difference was observed between the both doses (Figure 4). However, no particular amino acid
464 metabolism or carbohydrate metabolism was significantly affected by CBZ, as modulated proteins
465 were scattered in different metabolic pathways. Lipid metabolism was affected by CBZ exposure
466 mainly at the high dose and to a lesser extent at the low dose (Figure 4). Several peroxisomal
467 enzymes involved in fatty acid β -oxidation were up-modulated as illustrated in Table S3. Acyl-CoA
468 oxidase, one of the key enzymes involved in the β -oxidation process, was significantly up-modulated
469 (+230 %). Exposure to CBZ increased the fatty acid degradation that takes place in peroxisome and
470 affected the lipid homeostasis.

471

472 3.3. CBZ effects on metabolome related to proteogenomics data

473 Among the 294 signals selected from the blocks MetaboNEG and MetaboPOS, 82 were
474 annotated and reported in Table S1. Many signals were annotated at level 2, some of them with
475 several potential annotations, while 7 metabolites were identified at level 1. A total of 41 annotated
476 metabolites were significantly modulated (abundance modulation > 30 % and p-value < 0.05) at the
477 low dose (SCvsLD) (29 up-modulated and 12 down-modulated), while 33 annotated metabolites were
478 significantly modulated at the high dose (SCvsHD) (28 up-modulated and 5 down-modulated). The
479 specific metabolic pathway or class compound assigned to each metabolite is provided in Table S1.
480 Most of these metabolites belong to the amino acid metabolism, lipid metabolism and purine

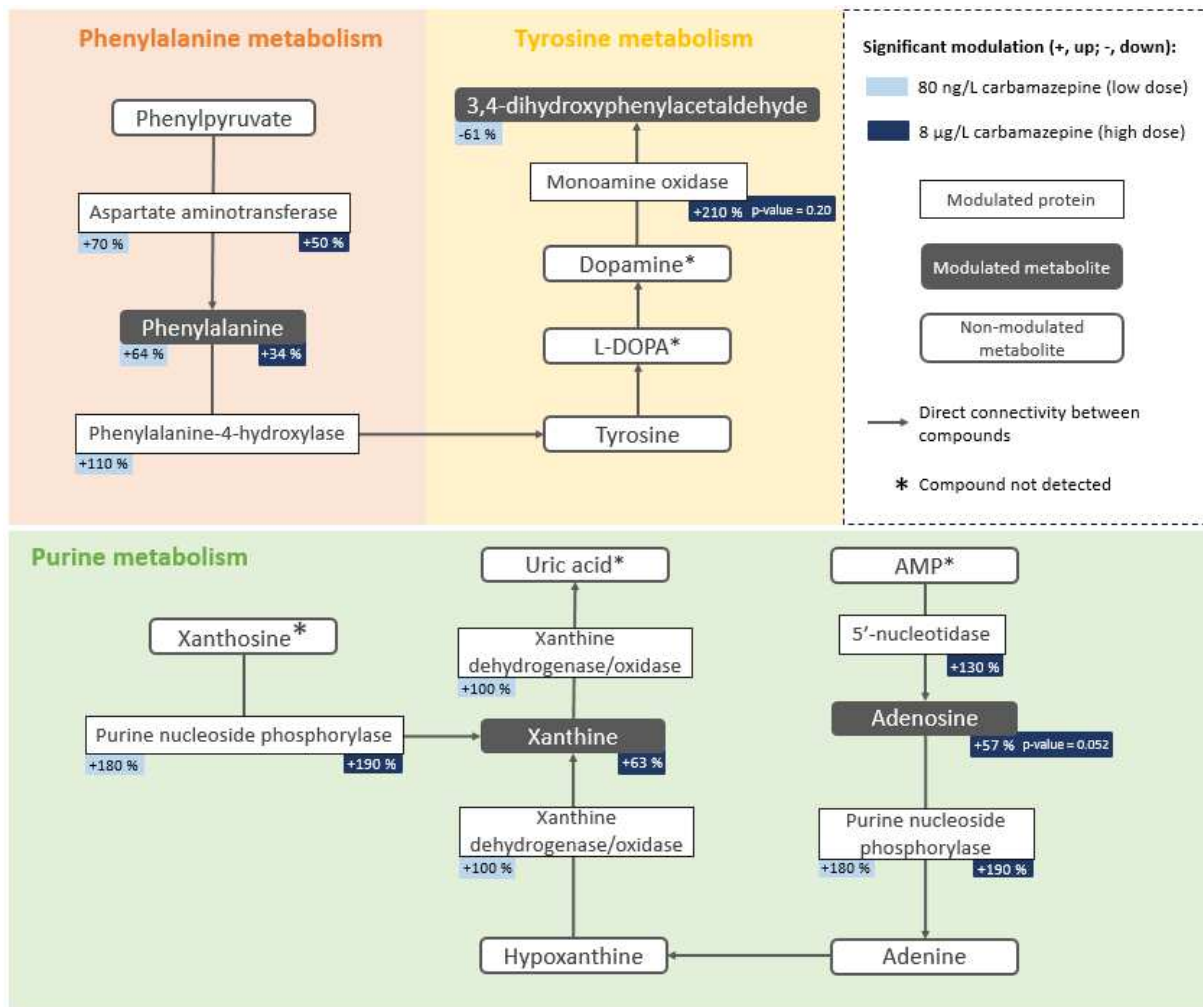
481 metabolism. What is interesting here, is to investigate the consistent modulation of metabolites in
482 accordance with protein modulations. As detailed in Table S4, several modulated proteins and
483 metabolites shared common metabolic pathways. When direct connections were investigated
484 between modulated proteins and metabolites, consistently affected pathways were observed for
485 purine metabolism, phenylalanine metabolism in relation to tyrosine, and lipid degradation. Detailed
486 metabolic pathways for purines, phenylalanine and tyrosine are illustrated in Figure 5.

487 At the low dose, modulation of phenylalanine (+64 %) was consistent with the up-modulation
488 of two enzymes, namely aspartate aminotransferase (+70 %) involved in the conversion of
489 phenylpyruvate to phenylalanine, and phenylalanine-4-hydroxylase (+110 %) which converts
490 phenylalanine to tyrosine which was not highlighted as modulated. Even if tyrosine, precursor of
491 catecholamines neurotransmitters (e.g., dopamine, metanephrine, norepinephrine, etc.), was not
492 modulated, the dopamine metabolites 3,4-dihydroxyphenylacetaldehyde (-61 %) and the
493 phenylalanine modulation indicates that the low dose of CBZ has modified the catecholamine
494 metabolism. At the high dose, phenylalanine up-modulation was maintained, as well as the up-
495 modulation of aspartate aminotransferase directly linked to this amino acid. Furthermore, a
496 modulation trend was observed for monoamine oxidase (+210 %; p-value = 0.198; high biological
497 variability) which catalyses the oxidative deamination of amines (i.e., dopamine, norepinephrine,
498 epinephrine, serotonin) although amine compounds were not detected or modulated at 3 days of
499 exposure.

500 Disturbances of purine metabolism were contrasted between the two CBZ doses (Figure 5).
501 While purine-nucleoside phosphorylase (+180 %) and xanthine dehydrogenase/oxidase (+100 %)
502 were up-modulated at the low dose, no related metabolite was affected. However, adenosine (+57
503 %; p-value = 0.052) and xanthine (+63 %) were up-modulated at the high dose consistently with an
504 up-modulation of purine-nucleoside phosphorylase (+190 %) and 5'-nucleotidase (+130 %). An up-
505 modulation of xanthine could be related to an increased nucleotides catabolism since it is the end
506 product just before its conversion to uric acid.

507 A large part of metabolites, modulated either at the low dose, the high dose or both,
508 belonged to the lipid metabolism. As reported in Table S1, the main compound classes of modulated
509 lipids were fatty acids, branched fatty acids, fatty esters, acyl carnitines and acyl glycines. A
510 disturbance of lipid metabolism is consistent with the proteogenomics data. For example, long-chain
511 specific acyl-CoA dehydrogenase, actively involved in fatty acid degradation in mitochondria, was up-
512 modulated at the low dose (+60 %). At the high dose, three different enzymes that complete the
513 fatty acid degradation in mitochondria and peroxisome were up-modulated (acyl-coenzyme A
514 oxidase 1; long-chain-fatty-acid--CoA ligase 4-like; peroxisomal bifunctional enzyme-like). In addition,
515 CBZ affected the arachidonic acid metabolism by the down-modulation of the two enzymes
516 prostaglandin-H2 D-isomerase/glutathione transferase (-60 %, low dose) and carbonyl reductase 1 (-
517 40 %, low dose; -70 % high dose) as well as a prostaglandin and a thromboxane metabolites (Table
518 S4). Arachidonic acid being the precursor of the eicosanoid family (prostaglandins, thromboxanes,
519 and leukotrienes), a disturbance of its metabolism could have physiological consequences regarding
520 the important role of eiconoid family in organisms.

521 Finally, several annotated metabolites corresponding to dipeptides (e.g. gamma-l-glutamyl-l-
522 leucine) were up-modulated at the low and/or high doses (Table S1). This is consistent with the
523 increase in proteins synthesis and degradation as dipeptides are catabolic products of proteins.



525

526 **Figure 5:** Metabolic pathways of phenylalanine, tyrosine and purine metabolisms represented by consistent changes in the
 527 levels of metabolites and proteins affected by the CBZ exposure at the low (80 ng/L) and high (8 µg/L) dose in the digestive
 528 gland of male mussel *Mytilus galloprovincialis*.

529 4. Discussion

530 The strategy of metabolomics and proteomics data fusion combining MCUVE-PLS and
531 consensus OPLS-DA, aimed to highlight metabolic and protein correlated signatures, and then to
532 study the possible relationships between these entities in response to the exposure of male *M.*
533 *galloprovincialis* to a low and high dose of CBZ. The two consensus OPLS-DA models, each comparing
534 the SC condition with either the low dose condition (SCvsLD) or the high dose condition (SCvsHD),
535 were found to be robust based on cross-validation. The combination of these two models was carried
536 out using a SUS-plot and allowed us to extract the most informative signals, related to common
537 modulation patterns shared by the two doses or specific to each of them. The links between proteins
538 and metabolites were then investigated using tools for visualizing metabolic pathways.

539 The interpretation of metabolomics data in combination with proteomics data is sometimes
540 difficult when it comes to explain changes from one omics level to another ⁶². The coordination
541 between the modulation of a metabolite and the modulation of a protein can be constrained by
542 feedback phenomena as well as by the time scale between them, or cannot be of the same
543 amplitude and thus not be detected. Indeed, the concentration of a metabolite can modulate the
544 expression of a gene, and changes in the expression of a gene can lead to an increase or decrease in
545 the concentration of a regulatory enzyme or protein, subsequently affecting the concentration of the
546 metabolite ⁶². Based on the simultaneous measurement of metabolite and transcript or protein
547 concentrations, different studies have reached contradictory conclusions on the coordination of the
548 observed changes between the different levels ⁶². Some studies have claimed that transcripts and
549 metabolites are substantially co-regulated ⁶³⁻⁶⁵, providing examples of consistent correlations
550 between biosynthetic enzymes and their products ⁶³. In contrast, other studies have shown that
551 transcript and metabolite profiles tend to behave differently ⁶⁶, and some have argued that
552 correlational approaches are not specific enough to draw conclusions about functionally related
553 genes and metabolites ^{67,68}. As our observations suggest, biochemical mechanisms probably lie
554 between these two conclusions. On the one hand, proteins and metabolites were co-regulated (e.g.

555 peroxisomal and mitochondrial enzymes and fatty acids, phenylalanine and phenylalanine-4-
556 hydroxylase, adenosine and purine nucleoside phosphorylase-like isoform X1, etc.). On the other
557 hand, changes in other protein and metabolite abundances seemed uncoordinated or isolated. In
558 addition to the feedback phenomena and time scales that may explain the latter cases, it is also
559 highly likely that partial access to the metabolome and proteome, as well as the lack of knowledge
560 about protein-metabolite and protein-protein interactions may explain these observations. However,
561 despite the lack of data related to bivalve mollusks, our integrative analysis of metabolomics and
562 proteomics data revealed promising results and consistent relationships between the two datasets in
563 response of the male mussel *M. galloprovincialis* to CBZ exposure.

564 Globally, the presented results indicated a metabolic and cellular stress in the digestive gland
565 of male mussels induced by CBZ at both concentrations (80 ng/L and 8 µg/L). As discussed hereafter,
566 this stress was revealed by different marker compounds of the lysosomal-autophagic system,
567 lysosomal membrane destabilization, overactivity of peroxisomal and mitochondrial enzymes,
568 apoptosis, or compounds involved in proteins synthesis and energy metabolism.

569 Autophagy induction following CBZ exposure was demonstrated in this study by numerous
570 modulated proteins. Autophagy clears aggregated and misfolded proteins as well as damaged
571 organelles via cytosolic sequestration and subsequent lysosomal degradation. One of the known
572 mechanisms of action of CBZ in mammals is the induction of autophagy by inhibition of inositol
573 monophosphatase (IMPase), leading to free inositol depletion and reduced myo-inositol-1,4,5-
574 triphosphate (IP3) ⁶⁹. Although autophagy and its induction is not well understood in bivalve
575 mollusks ⁷⁰, autophagy is a mechanism widely conserved in eukaryotes. Our findings showed a
576 significant modulation of IMPase at both exposure doses. It means that CBZ can act on the
577 intracellular inositol levels with consequences for the autophagy regulation, although inositol or IP3
578 were not detected by the metabolomics analysis. Another hypothesis can be put forward regarding
579 the induction of autophagy. Endoplasmic reticulum (ER) stress (e.g., accumulation of misfolded
580 proteins, change in Ca²⁺ level) is known as a particularly efficient stimulus for autophagy ⁷¹. This study

581 demonstrated an ER stress through the up-modulation of protein synthesis and the potential
582 increase in misfolded proteins. ER stress was also highlighted by a high up-modulation of bax
583 inhibitor-1 and sarco/endoplasmic reticulum calcium ATPase at both CBZ doses. Sarco/endoplasmic
584 reticulum calcium ATPase is a Ca²⁺ transport protein of the ER membrane maintaining the low
585 cytosolic calcium level that enable a vast array of signaling pathways and physiological processes ⁷².
586 Bax inhibitor-1 is an ER-located protein, with anti-apoptotic functions, involved in the suppression of
587 intrinsic cell death mediated by ER stress or ER calcium release (see references in ⁷³). Evidences were
588 provided on the dual role of Bax inhibitor-1 to regulate both autophagy and apoptosis, two closely
589 related homeostatic processes ⁷³. Further research is then needed to elucidate the mechanism of
590 action of CBZ in bivalve mollusks, triggering autophagy either via depletion of inositol or by the
591 induction of ER stress.

592 In response to exposure in bivalves, lysosomes contribute to the degradation and
593 detoxification of contaminants through different enzymes ⁷⁴. Among these enzymes, cathepsins are
594 often involved in the detoxification of metals or organic contaminants ²². In our study, the exposure
595 at the low and high doses induced an up-modulation of cathepsin B and a cathepsin-like protein-4,
596 and a down-modulation of cathepsin L. An over-expression of the gene coding for cathepsin L in the
597 digestive glands of *M. galloprovincialis* mussels, exposed for 3 days to 6.3 µg/L CBZ (close to the
598 present study exposure conditions) was reported in a recent study ²². Exposure of the marine bivalve
599 *Ruditapes philippinarum* to 1 µg/L CBZ for 28 days also resulted in over-expression of the same
600 gene ²¹. Changes in cathepsin abundance may reflect a general up-regulation of lysosomal proteolysis
601 due to either damage to cellular proteins or direct effects on protease activity due to CBZ
602 sequestration in lysosomes. However, an elevated lysosomal activity or sequestration of
603 contaminants in lysosomes can affect the lysosomal integrity (e.g. membrane permeability, size of
604 lysosome) ^{74,75}. In marine bivalves, β-glucuronidase is even used as lysosomal enzymatic markers of
605 changes in membrane permeability and lysosome size ^{74,76}. In our study, significant up-modulation of
606 β-glucuronidase was observed at the low (+210 %; p-value = 0.004) and high dose (+130 %; p-value =

607 0.034), although it was not selected by MCUVE-PLS. A modification of the membrane permeability of
608 the lysosomes or their morphology is possible at both exposure doses. At comparable doses of CBZ
609 (0.1 µg/L and 10 µg/L) but a longer exposure time (7 days), Martin-Diaz et al.²³ measured a dose-
610 dependent decrease in the stability of the lysosome membranes of haemocytes, collected from the
611 digestive gland of *M. galloprovincialis*. As a consequence, hydrolytic lysosomal enzymes can be
612 released in the cytosol causing severe cellular damages and even cell death⁷⁷.

613 Peroxisomes and mitochondria play a very important role in the phenomena of β-oxidation
614 of fatty acids to maintain lipid homeostasis in eukaryotic cells⁷⁸. These enzymatic reactions produce
615 reactive oxygen species (ROS) such as hydrogen peroxide (H₂O₂), which is then degraded by
616 catalase⁷⁹. In our study, an up-modulation of the peroxisomal enzymes responsible for the β-
617 oxidation of saturated and unsaturated fatty acids (e.g. acyl-CoA oxidase; long-chain acyl-CoA
618 synthetase; peroxisomal multifunctional enzyme type 2 isoform X2) was observed, mainly at the high
619 CBZ dose, as well as a slight up-modulation of catalase. In conjunction with this, the metabolomics
620 data also showed a disturbance in the metabolism of lipids and especially fatty acids. It also includes
621 a disturbance of arachidonic acid metabolism, precursor of eicosanoids, playing an important role in
622 bivalves reproduction and others physiological processes⁸⁰. In response to a number of endogenous
623 compounds and xenobiotics, peroxisomes can undergo massive proliferation. This phenomenon is
624 usually accompanied by the induction of certain peroxisomal enzyme activities, particularly those of
625 the fatty acid β-oxidation system, while catalase may not be induced or weakly induced^{79,81}.
626 Consequently, peroxisome proliferation is considered as a potential source of oxidative stress for
627 cells, since ROS-producing enzymes are induced to a greater extent than the catalase capable of
628 detoxifying ROS^{82,83}, which could be the case in our study. Although the induction of peroxisomal
629 proliferation has already been observed in the cells of the digestive gland of *M. galloprovincialis* in
630 response to contaminants⁸⁴, to our knowledge this phenomenon has not been described in
631 invertebrates exposed to CBZ. More targeted measurements on the numerical and volume density of
632 peroxisomes and on the enzymatic activity of acyl-CoA oxidase would make it possible to verify this

633 hypothesis⁸⁴. Peroxisome (or even peroxisome proliferation) dysfunction can cause an unbalanced
634 ROS homeostasis leading to cellular damages and cell death⁷⁸.

635 In this study, organelles (e.g. lysosome, peroxysome and endoplasmic reticulum) stress
636 and/or dysfunction triggered by CBZ exposure, as well as possible oxidative stress, can induce
637 apoptosis⁸⁵. This hypothesis is supported by several proteins involved in apoptotic processes,
638 modulated at the low or high dose, such as TNF ligand-like 1, TNF ligand superfamily member 10,
639 caspase 2, cathepsin B, apoptosis-inducing factor 3 isoform X1, mitogen-activated protein kinase
640 kinase 1, and quinone oxidoreductase PIG3-like isoform X2^{86–91}. Although apoptosis was not directly
641 measured in mollusks exposed to CBZ, Mezzelani et al.⁹² observed several up-regulated genes with a
642 role in apoptotic processes after *M. galloprovincialis* exposure to 1 µg/L CBZ (28 days). Furthermore,
643 this programmed cell death was observed in the Chinese rare minnows *Gobiocypris rarus* exposed 28
644 days at 1, 10 and 100 µg/L CBZ⁹³. After a 3-days exposure, we were probably at an early stage of the
645 apoptosis signaling pathway. Prolonged exposure to CBZ would eventually lead to programmed cell
646 death, even at environmentally relevant concentrations.

647 The general metabolic and cellular stress in digestive gland of male mussels triggered by CBZ
648 exposure can also be demonstrated by an increase in protein turnover. This turnover was marked by
649 an increase in both protein synthesis (e.g., increasing numbers of ribosomal proteins and proteins
650 from endoplasmic reticulum) and catabolism (e.g., increasing numbers of dipeptides, catabolic
651 products of proteins). Catabolic processes are thought to remove damaged proteins while the
652 synthesis of new and protective proteins is vital for the preservation of cellular homeostasis during
653 CBZ-induced stress. However, faced with environmental stressors or pollution, mussels generally
654 adopt a strategy of depressing protein synthesis to protect themselves⁹⁴. Organisms limit protein
655 synthesis by storing inactive ribosomes that are rapidly reactivated when conditions improve. In the
656 present study, it would be interesting to check whether ribosomal proteins are active in the
657 translation process or whether they are stored for inactive ribosomes assembly. In any case, both
658 strategies reveal a general stress induced by CBZ exposure at environmental concentrations.

659 The integrated analysis of proteomics and metabolomics data provided a detailed view of the
660 cellular and metabolic processes modulated in response to CBZ, indicating a general state of stress in
661 the cells of the digestive gland of male *M. galloprovincialis*. Our findings provide preliminary results
662 on CBZ mechanism of action related to autophagy induction in bivalve mollusks, either by inositol
663 depletion or ER stress. Furthermore, as the induction of oxidative stress is the most frequently
664 reported effect of CBZ in non-target organisms, this study could provide more details on the causes
665 of this stress. Indeed, oxidative stress can be triggered following a possible destabilization of the
666 lysosomal membranes, already demonstrated by other studies, but also through an enzymatic
667 overactivity of the peroxisomes (or even peroxisome proliferation), of which our results provide the
668 first evidence in *M. galloprovincialis*. As supported by others studies, ROS production and cellular
669 damages could lead to programmed cell death. Our results show several modulated proteins
670 involved in apoptotic processes. These cytotoxic effects generated by CBZ could also explain the
671 decrease in cell viability observed in studies conducted on mussel haemocytes. As example, decrease
672 in cell viability was measured in *M. galloprovincialis* haemocytes treated for 1 hour at different CBZ
673 concentrations (0.01; 0.1; 1; 10 and 100 µg/L)²⁴ or on haemocytes of the freshwater mussel
674 *Dreissena polymorpha* from 96h of treatment at the lowest CBZ dose tested 1 µg/L⁹⁷. Induction of
675 cellular death or a decrease in cell viability would result in a weakening of the mussel immune system
676^{24,97}. The general stress triggered by CBZ was initiated as early as 3 days of exposure to an
677 environmental concentration (80 ng/L) but more intensively at the higher dose (8 µg/L). It would be
678 interesting to check whether prolonged exposure to the low dose would induce the level of stress
679 reached at the high dose, or whether organisms can adapt to prolonged exposure by developing
680 strategies to mitigate the toxicity. Further research is also needed to decipher the molecular initiating
681 events leading to the overall metabolic and cellular stresses observed in this study.

682

683 **Declaration of competing interest**

684 We declare that there is no conflict of interest for this paper.

685

686 **Acknowledgement & Funding**

687 This research was funded by the Agence Nationale de la Recherche (IMAP ANR-16-CE34-
688 0006-01). The doctoral fellowship of Thibaut Dumas was financially supported by the Agence
689 Nationale de la Recherche (IMAP ANR-16-CE34-0006-01). The authors thank the PONTEM (Platform
690 Of Non-Target Environmental Metabolomics) platform from the consortium facilities MAMMA
691 (Montpellier Alliance for Metabolomics and Metabolism Analysis). Technical assistance of Céline
692 Roques and Bénédicte Marion (Institut des Biomolécules Max Mousseron, Montpellier, France) and
693 Guylaine Miotello (Atomic Energy and Alternative Energies Commission, CEA, Bagnols-sur-Cèze,
694 France) is gratefully acknowledged.

695

696 **Appendix A. Supplementary Data**

697 The following are available online at [XXXX], Figure S1: Folding, sorting and degradation
698 processes disrupted by exposure to low and high doses of carbamazepine (KEGG pathway). Table S1:
699 Annotation and identification of relevant metabolites selected according to the SUS-plot, modulated
700 by CBZ exposure in male mussels either at the low dose, high dose, or both. Table S2: Annotation of
701 relevant proteins selected according to the SUS-plot, modulated by CBZ exposure in male mussels
702 either at the low dose, high dose, or both. Table S3: Relevant proteins selected by the models,
703 involved in the transport and catabolism cellular process. Table S4: Modulated metabolites and
704 proteins involved in common metabolic pathways.

705

706 **References**

- 707 (1) Margot, J.; Rossi, L.; Barry, D. A.; Holliger, C. A Review of the Fate of Micropollutants in
708 Wastewater Treatment Plants. *WIREs Water* **2015**, *2* (5), 457–487.
709 <https://doi.org/10.1002/wat2.1090>.
- 710 (2) Benotti, M. J.; Brownawell, B. J. Microbial Degradation of Pharmaceuticals in Estuarine and
711 Coastal Seawater. *Environ. Pollut.* **2009**, *157* (3), 994–1002.
712 <https://doi.org/10.1016/j.envpol.2008.10.009>.

- 713 (3) Calisto, V.; Domingues, M. R. M.; Erny, G. L.; Esteves, V. I. Direct Photodegradation of
714 Carbamazepine Followed by Micellar Electrokinetic Chromatography and Mass Spectrometry.
715 *Water Res.* **2011**, *45* (3), 1095–1104. <https://doi.org/10.1016/j.watres.2010.10.037>.
- 716 (4) Clara, M.; Strenn, B.; Kreuzinger, N. Carbamazepine as a Possible Anthropogenic Marker in the
717 Aquatic Environment: Investigations on the Behaviour of Carbamazepine in Wastewater
718 Treatment and during Groundwater Infiltration. *Water Res.* **2004**, *38* (4), 947–954.
719 <https://doi.org/10.1016/j.watres.2003.10.058>.
- 720 (5) Hai, F. I.; Yang, S.; Asif, M. B.; Sencadas, V.; Shawkat, S.; Sanderson-Smith, M.; Gorman, J.; Xu,
721 Z.-Q.; Yamamoto, K. Carbamazepine as a Possible Anthropogenic Marker in Water:
722 Occurrences, Toxicological Effects, Regulations and Removal by Wastewater Treatment
723 Technologies. *Water* **2018**, *10* (2), 107. <https://doi.org/10.3390/w10020107>.
- 724 (6) Fabbri, E.; Franzellitti, S. Human Pharmaceuticals in the Marine Environment: Focus on
725 Exposure and Biological Effects in Animal Species. *Environ. Toxicol. Chem.* **2016**, *35* (4), 799–
726 812. <https://doi.org/10.1002/etc.3131>.
- 727 (7) Mezzelani, M.; Gorbi, S.; Regoli, F. Pharmaceuticals in the Aquatic Environments: Evidence of
728 Emerged Threat and Future Challenges for Marine Organisms. *Mar. Environ. Res.* **2018**, *140*,
729 41–60. <https://doi.org/10.1016/j.marenvres.2018.05.001>.
- 730 (8) Prichard, E.; Granek, E. F. Effects of Pharmaceuticals and Personal Care Products on Marine
731 Organisms: From Single-Species Studies to an Ecosystem-Based Approach. *Environ. Sci. Pollut.*
732 *Res. Int.* **2016**, *23* (22), 22365–22384. <https://doi.org/10.1007/s11356-016-7282-0>.
- 733 (9) Ebele, A. J.; Abou-Elwafa Abdallah, M.; Harrad, S. Pharmaceuticals and Personal Care Products
734 (PPCPs) in the Freshwater Aquatic Environment. *Emerg. Contam.* **2017**, *3* (1), 1–16.
735 <https://doi.org/10.1016/j.emcon.2016.12.004>.
- 736 (10) Ternes, T. A.; Herrmann, N.; Bonerz, M.; Knacker, T.; Siegrist, H.; Joss, A. A Rapid Method to
737 Measure the Solid–Water Distribution Coefficient (Kd) for Pharmaceuticals and Musk
738 Fragrances in Sewage Sludge. *Water Res.* **2004**, *38* (19), 4075–4084.
739 <https://doi.org/10.1016/j.watres.2004.07.015>.
- 740 (11) Zhang, Y.; Geißen, S.-U.; Gal, C. Carbamazepine and Diclofenac: Removal in Wastewater
741 Treatment Plants and Occurrence in Water Bodies. *Chemosphere* **2008**, *73* (8), 1151–1161.
742 <https://doi.org/10.1016/j.chemosphere.2008.07.086>.
- 743 (12) Arpin-Pont, L.; Bueno, M. J. M.; Gomez, E.; Fenet, H. Occurrence of PPCPs in the Marine
744 Environment: A Review. *Environ. Sci. Pollut. Res.* **2016**, *23* (6), 4978–4991.
745 <https://doi.org/10.1007/s11356-014-3617-x>.
- 746 (13) McEneff, G.; Barron, L.; Kelleher, B.; Paull, B.; Quinn, B. A Year-Long Study of the Spatial
747 Occurrence and Relative Distribution of Pharmaceutical Residues in Sewage Effluent,
748 Receiving Marine Waters and Marine Bivalves. *Sci. Total Environ.* **2014**, *476*, 317–326.
749 <https://doi.org/10.1016/j.scitotenv.2013.12.123>.
- 750 (14) Alvarez-Muñoz, D.; Huerta, B.; Fernandez-Tejedor, M.; Rodríguez-Mozaz, S.; Barceló, D. Multi-
751 Residue Method for the Analysis of Pharmaceuticals and Some of Their Metabolites in
752 Bivalves. *Talanta* **2015**, *136*, 174–182. <https://doi.org/10.1016/j.talanta.2014.12.035>.
- 753 (15) Martínez Bueno, M. J.; Boillot, C.; Fenet, H.; Chiron, S.; Casellas, C.; Gómez, E. Fast and Easy
754 Extraction Combined with High Resolution-Mass Spectrometry for Residue Analysis of Two
755 Anticonvulsants and Their Transformation Products in Marine Mussels. *J. Chromatogr. A* **2013**,
756 *1305*, 27–34. <https://doi.org/10.1016/j.chroma.2013.06.071>.
- 757 (16) Wille, K.; Kiebooms, J. A. L.; Claessens, M.; Rappé, K.; Vanden Bussche, J.; Noppe, H.; Van
758 Praet, N.; De Wulf, E.; Van Caeter, P.; Janssen, C. R.; De Brabander, H. F.; Vanhaecke, L.
759 Development of Analytical Strategies Using U-HPLC-MS/MS and LC-ToF-MS for the
760 Quantification of Micropollutants in Marine Organisms. *Anal. Bioanal. Chem.* **2011**, *400* (5),
761 1459–1472. <https://doi.org/10.1007/s00216-011-4878-6>.
- 762 (17) Boillot, C.; Martínez Bueno, M. J.; Munaron, D.; Le Dreau, M.; Mathieu, O.; David, A.; Fenet,
763 H.; Casellas, C.; Gomez, E. In Vivo Exposure of Marine Mussels to Carbamazepine and 10-

- 764 Hydroxy-10,11-Dihydro-Carbamazepine: Bioconcentration and Metabolization. *Sci. Total*
765 *Environ.* **2015**, 532, 564–570. <https://doi.org/10.1016/j.scitotenv.2015.05.067>.
- 766 (18) Almeida, A.; Calisto, V.; Esteves, V. I.; Schneider, R. J.; Soares, A. M. V. M.; Figueira, E.; Freitas,
767 R. Presence of the Pharmaceutical Drug Carbamazepine in Coastal Systems: Effects on
768 Bivalves. *Aquat. Toxicol. Amst. Neth.* **2014**, 156, 74–87.
769 <https://doi.org/10.1016/j.aquatox.2014.08.002>.
- 770 (19) Almeida, Â.; Esteves, V. I.; Soares, A. M. V. M.; Freitas, R. Effects of Carbamazepine in Bivalves:
771 A Review; Reviews of Environmental Contamination and Toxicology; Springer International
772 Publishing: Cham, 2020; pp 1–19. https://doi.org/10.1007/398_2020_51.
- 773 (20) Aguirre-Martínez, G. V.; Buratti, S.; Fabbr, E.; DelValls, A. T.; Martín-Díaz, M. L. Using
774 Lysosomal Membrane Stability of Haemocytes in Ruditapes Philippinarum as a Biomarker of
775 Cellular Stress to Assess Contamination by Caffeine, Ibuprofen, Carbamazepine and
776 Novobiocin. *J. Environ. Sci. China* **2013**, 25 (7), 1408–1418. [https://doi.org/10.1016/s1001-](https://doi.org/10.1016/s1001-0742(12)60207-1)
777 [0742\(12\)60207-1](https://doi.org/10.1016/s1001-0742(12)60207-1).
- 778 (21) Almeida, Â.; Freitas, R.; Calisto, V.; Esteves, V. I.; Schneider, R. J.; Soares, A. M. V. M.; Figueira,
779 E.; Campos, B.; Barata, C. Effects of Carbamazepine and Cetirizine under an Ocean
780 Acidification Scenario on the Biochemical and Transcriptome Responses of the Clam Ruditapes
781 Philippinarum. *Environ. Pollut.* **2018**, 235, 857–868.
782 <https://doi.org/10.1016/j.envpol.2017.12.121>.
- 783 (22) Brandts, I.; Teles, M.; Gonçalves, A. P.; Barreto, A.; Franco-Martinez, L.; Tvarijonaviciute, A.;
784 Martins, M. A.; Soares, A. M. V. M.; Tort, L.; Oliveira, M. Effects of Nanoplastics on Mytilus
785 Galloprovincialis after Individual and Combined Exposure with Carbamazepine. *Sci. Total*
786 *Environ.* **2018**, 643, 775–784. <https://doi.org/10.1016/j.scitotenv.2018.06.257>.
- 787 (23) Martin-Diaz, L.; Franzellitti, S.; Buratti, S.; Valbonesi, P.; Capuzzo, A.; Fabbri, E. Effects of
788 Environmental Concentrations of the Antiepileptic Drug Carbamazepine on Biomarkers and
789 CAMP-Mediated Cell Signaling in the Mussel Mytilus Galloprovincialis. *Aquat. Toxicol. Amst.*
790 *Neth.* **2009**, 94 (3), 177–185. <https://doi.org/10.1016/j.aquatox.2009.06.015>.
- 791 (24) Tsiaka, P.; Tsarpali, V.; Ntaikou, I.; Kostopoulou, M. N.; Lyberatos, G.; Dailianis, S.
792 Carbamazepine-Mediated pro-Oxidant Effects on the Unicellular Marine Algal Species
793 Dunaliella Tertiolecta and the Hemocytes of Mussel Mytilus Galloprovincialis. *Ecotoxicology*
794 **2013**, 22 (8), 1208–1220. <https://doi.org/10.1007/s10646-013-1108-3>.
- 795 (25) Aguirre-Martínez, G. V.; DelValls, A. T.; Laura Martín-Díaz, M. Yes, Caffeine, Ibuprofen,
796 Carbamazepine, Novobiocin and Tamoxifen Have an Effect on Corbicula Fluminea (Müller,
797 1774). *Ecotoxicol. Environ. Saf.* **2015**, 120, 142–154.
798 <https://doi.org/10.1016/j.ecoenv.2015.05.036>.
- 799 (26) Franzellitti, S.; Balbi, T.; Montagna, M.; Fabbri, R.; Valbonesi, P.; Fabbri, E.; Canesi, L.
800 Phenotypical and Molecular Changes Induced by Carbamazepine and Propranolol on Larval
801 Stages of Mytilus Galloprovincialis. *Chemosphere* **2019**, 234, 962–970.
802 <https://doi.org/10.1016/j.chemosphere.2019.06.045>.
- 803 (27) Freitas, R.; Almeida, Â.; Calisto, V.; Velez, C.; Moreira, A.; Schneider, R. J.; Esteves, V. I.; Wrona,
804 F. J.; Figueira, E.; Soares, A. M. V. M. The Impacts of Pharmaceutical Drugs under Ocean
805 Acidification: New Data on Single and Combined Long-Term Effects of Carbamazepine on
806 Scrobicularia Plana. *Sci. Total Environ.* **2016**, 541, 977–985.
807 <https://doi.org/10.1016/j.scitotenv.2015.09.138>.
- 808 (28) Canzler, S.; Schor, J.; Busch, W.; Schubert, K.; Rolle-Kampczyk, U. E.; Seitz, H.; Kamp, H.; von
809 Bergen, M.; Buesen, R.; Hackermüller, J. Prospects and Challenges of Multi-Omics Data
810 Integration in Toxicology. *Arch. Toxicol.* **2020**, 94 (2), 371–388.
811 <https://doi.org/10.1007/s00204-020-02656-y>.
- 812 (29) Pinu, F. R.; Beale, D. J.; Paten, A. M.; Kouremenos, K.; Swarup, S.; Schirra, H. J.; Wishart, D.
813 Systems Biology and Multi-Omics Integration: Viewpoints from the Metabolomics Research
814 Community. *Metabolites* **2019**, 9 (4). <https://doi.org/10.3390/metabo9040076>.

- 815 (30) Chen, H.; Diao, X.; Wang, H.; Zhou, H. An Integrated Metabolomic and Proteomic Study of
816 Toxic Effects of Benzo[a]Pyrene on Gills of the Pearl Oyster *Pinctada Martensii*. *Ecotoxicol.*
817 *Environ. Saf.* **2018**, *156*, 330–336. <https://doi.org/10.1016/j.ecoenv.2018.03.040>.
- 818 (31) Ji, C.; Li, F.; Wang, Q.; Zhao, J.; Sun, Z.; Wu, H. An Integrated Proteomic and Metabolomic
819 Study on the Gender-Specific Responses of Mussels *Mytilus Galloprovincialis*
820 to Tetrabromobisphenol A (TBBPA). *Chemosphere* **2016**, *144*, 527–539.
821 <https://doi.org/10.1016/j.chemosphere.2015.08.052>.
- 822 (32) Sun, J.; Zhou, Q.; Hu, X. Integrating Multi-Omics and Regular Analyses Identifies the Molecular
823 Responses of Zebrafish Brains to Graphene Oxide: Perspectives in Environmental Criteria.
824 *Ecotoxicol. Environ. Saf.* **2019**, *180*, 269–279. <https://doi.org/10.1016/j.ecoenv.2019.05.011>.
- 825 (33) Wu, C.; Zhou, F.; Ren, J.; Li, X.; Jiang, Y.; Ma, S. A Selective Review of Multi-Level Omics Data
826 Integration Using Variable Selection. *High-Throughput* **2019**, *8* (1), 4.
827 <https://doi.org/10.3390/ht8010004>.
- 828 (34) Steinmetz, V.; Sévila, F.; Bellon-Maurel, V. A Methodology for Sensor Fusion Design:
829 Application to Fruit Quality Assessment. *J. Agric. Eng. Res.* **1999**, *74* (1), 21–31.
830 <https://doi.org/10.1006/jaer.1999.0428>.
- 831 (35) Boccard, J.; Rudaz, S. Harnessing the Complexity of Metabolomic Data with Chemometrics. *J.*
832 *Chemom.* **2014**, *28* (1), 1–9. <https://doi.org/10.1002/cem.2567>.
- 833 (36) Cai, W.; Li, Y.; Shao, X. A Variable Selection Method Based on Uninformative Variable
834 Elimination for Multivariate Calibration of Near-Infrared Spectra. *Chemom. Intell. Lab. Syst.*
835 **2008**, *90* (2), 188–194. <https://doi.org/10.1016/j.chemolab.2007.10.001>.
- 836 (37) Boccard, J.; Rutledge, D. N. A Consensus Orthogonal Partial Least Squares Discriminant
837 Analysis (OPLS-DA) Strategy for Multiblock Omics Data Fusion. *Anal. Chim. Acta* **2013**, *769*, 30–
838 39. <https://doi.org/10.1016/j.aca.2013.01.022>.
- 839 (38) Bonnefille, B.; Gomez, E.; Alali, M.; Rosain, D.; Fenet, H.; Courant, F. Metabolomics
840 Assessment of the Effects of Diclofenac Exposure on *Mytilus Galloprovincialis*: Potential
841 Effects on Osmoregulation and Reproduction. *Sci. Total Environ.* **2018**, *613–614*, 611–618.
842 <https://doi.org/10.1016/j.scitotenv.2017.09.146>.
- 843 (39) Dumas, T.; Bonnefille, B.; Gomez, E.; Boccard, J.; Castro, N. A.; Fenet, H.; Courant, F.
844 Metabolomics Approach Reveals Disruption of Metabolic Pathways in the Marine Bivalve
845 *Mytilus Galloprovincialis* Exposed to a WWTP Effluent Extract. *Sci. Total Environ.* **2020**, *712*,
846 136551. <https://doi.org/10.1016/j.scitotenv.2020.136551>.
- 847 (40) Want, E. J.; Masson, P.; Michopoulos, F.; Wilson, I. D.; Theodoridis, G.; Plumb, R. S.; Shockcor,
848 J.; Loftus, N.; Holmes, E.; Nicholson, J. K. Global Metabolic Profiling of Animal and Human
849 Tissues via UPLC-MS. *Nat. Protoc.* **2013**, *8* (1), 17–32. <https://doi.org/10.1038/nprot.2012.135>.
- 850 (41) Dumas, T.; Boccard, J.; Gomez, E.; Fenet, H.; Courant, F. Multifactorial Analysis of
851 Environmental Metabolomic Data in Ecotoxicology: Wild Marine Mussel Exposed to WWTP
852 Effluent as a Case Study. *Metabolites* **2020**, *10* (7), 269.
853 <https://doi.org/10.3390/metabo10070269>.
- 854 (42) Kessner, D.; Chambers, M.; Burke, R.; Agus, D.; Mallick, P. ProteoWizard: Open Source
855 Software for Rapid Proteomics Tools Development. *Bioinformatics* **2008**, *24* (21), 2534–2536.
856 <https://doi.org/10.1093/bioinformatics/btn323>.
- 857 (43) Smith, C. A.; Want, E. J.; O’Maille, G.; Abagyan, R.; Siuzdak, G. XCMS: Processing Mass
858 Spectrometry Data for Metabolite Profiling Using Nonlinear Peak Alignment, Matching, and
859 Identification. *Anal. Chem.* **2006**, *78* (3), 779–787. <https://doi.org/10.1021/ac051437y>.
- 860 (44) Kuhl, C.; Tautenhahn, R.; Böttcher, C.; Larson, T. R.; Neumann, S. CAMERA: An Integrated
861 Strategy for Compound Spectra Extraction and Annotation of Liquid Chromatography/Mass
862 Spectrometry Data Sets. *Anal. Chem.* **2012**, *84* (1), 283–289.
863 <https://doi.org/10.1021/ac202450g>.
- 864 (45) Wishart, D. S.; Jewison, T.; Guo, A. C.; Wilson, M.; Knox, C.; Liu, Y.; Djoumbou, Y.; Mandal, R.;
865 Aziat, F.; Dong, E.; Bouatra, S.; Sinelnikov, I.; Arndt, D.; Xia, J.; Liu, P.; Yallou, F.; Bjorn Dahl, T.;
866 Perez-Pineiro, R.; Eisner, R.; Allen, F.; Neveu, V.; Greiner, R.; Scalbert, A. HMDB 3.0—The

- 867 Human Metabolome Database in 2013. *Nucleic Acids Res.* **2013**, *41* (D1), D801–D807.
868 <https://doi.org/10.1093/nar/gks1065>.
- 869 (46) Fahy, E.; Subramaniam, S.; Murphy, R. C.; Nishijima, M.; Raetz, C. R. H.; Shimizu, T.; Spener, F.;
870 Meer, G. van; Wakelam, M. J. O.; Dennis, E. A. Update of the LIPID MAPS Comprehensive
871 Classification System for Lipids. *J. Lipid Res.* **2009**, *50* (Supplement), S9–S14.
872 <https://doi.org/10.1194/jlr.R800095-JLR200>.
- 873 (47) Blaženović, I.; Kind, T.; Ji, J.; Fiehn, O. Software Tools and Approaches for Compound
874 Identification of LC-MS/MS Data in Metabolomics. *Metabolites* **2018**, *8* (2), 31.
875 <https://doi.org/10.3390/metabo8020031>.
- 876 (48) Liebisch, G.; Fahy, E.; Aoki, J.; Dennis, E. A.; Durand, T.; Ejsing, C. S.; Fedorova, M.; Feussner, I.;
877 Griffiths, W. J.; Köfeler, H.; Merrill, A. H.; Murphy, R. C.; O'Donnell, V. B.; Oskolkova, O.;
878 Subramaniam, S.; Wakelam, M. J. O.; Spener, F. Update on LIPID MAPS Classification,
879 Nomenclature, and Shorthand Notation for MS-Derived Lipid Structures. *J. Lipid Res.* **2020**, *61*
880 (12), 1539–1555. <https://doi.org/10.1194/jlr.S120001025>.
- 881 (49) Hayoun, K.; Gouveia, D.; Grenga, L.; Pible, O.; Armengaud, J.; Alpha-Bazin, B. Evaluation of
882 Sample Preparation Methods for Fast Proteotyping of Microorganisms by Tandem Mass
883 Spectrometry. *Front. Microbiol.* **2019**, *10*, 1985. <https://doi.org/10.3389/fmicb.2019.01985>.
- 884 (50) Trapp, J.; Armengaud, J.; Pible, O.; Gaillard, J.-C.; Abbaci, K.; Habtoul, Y.; Chaumot, A.; Geffard,
885 O. Proteomic Investigation of Male Gammarus Fossarum, a Freshwater Crustacean, in
886 Response to Endocrine Disruptors. *J. Proteome Res.* **2015**, *14* (1), 292–303.
887 <https://doi.org/10.1021/pr500984z>.
- 888 (51) Hartmann, E. M.; Allain, F.; Gaillard, J.-C.; Pible, O.; Armengaud, J. Taking the Shortcut for
889 High-Throughput Shotgun Proteomic Analysis of Bacteria. In *Host-Bacteria Interactions:
890 Methods and Protocols*; Vergunst, A. C., O'Callaghan, D., Eds.; Methods in Molecular Biology;
891 Springer: New York, NY, 2014; pp 275–285. https://doi.org/10.1007/978-1-4939-1261-2_16.
- 892 (52) Klein, G.; Mathé, C.; Biola-Clier, M.; Devineau, S.; Drouineau, E.; Hatem, E.; Marichal, L.;
893 Alonso, B.; Gaillard, J.-C.; Lagniel, G.; Armengaud, J.; Carrière, M.; Chédin, S.; Boulard, Y.; Pin,
894 S.; Renault, J.-P.; Aude, J.-C.; Labarre, J. RNA-Binding Proteins Are a Major Target of Silica
895 Nanoparticles in Cell Extracts. *Nanotoxicology* **2016**, *10* (10), 1555–1564.
896 <https://doi.org/10.1080/17435390.2016.1244299>.
- 897 (53) Haas, B. J.; Papanicolaou, A.; Yassour, M.; Grabherr, M.; Blood, P. D.; Bowden, J.; Couger, M.
898 B.; Eccles, D.; Li, B.; Lieber, M.; MacManes, M. D.; Ott, M.; Orvis, J.; Pochet, N.; Strozzi, F.;
899 Weeks, N.; Westerman, R.; William, T.; Dewey, C. N.; Henschel, R.; LeDuc, R. D.; Friedman, N.;
900 Regev, A. De Novo Transcript Sequence Reconstruction from RNA-Seq Using the Trinity
901 Platform for Reference Generation and Analysis. *Nat. Protoc.* **2013**, *8* (8), 1494–1512.
902 <https://doi.org/10.1038/nprot.2013.084>.
- 903 (54) Cogne, Y.; Degli-Esposti, D.; Pible, O.; Gouveia, D.; François, A.; Bouchez, O.; Eché, C.; Ford, A.;
904 Geffard, O.; Armengaud, J.; Chaumot, A.; Almunia, C. De Novo Transcriptomes of 14
905 Gammarid Individuals for Proteogenomic Analysis of Seven Taxonomic Groups. *Sci. Data* **2019**,
906 *6* (1), 184. <https://doi.org/10.1038/s41597-019-0192-5>.
- 907 (55) Wright, J. C.; Choudhary, J. S. DecoyPyrat: Fast Non-Redundant Hybrid Decoy Sequence
908 Generation for Large Scale Proteomics. *J. Proteomics Bioinform.* **2016**, *9* (6), 176–180.
909 <https://doi.org/10.4172/jpb.1000404>.
- 910 (56) Trapp, J.; Gouveia, D.; Almunia, C.; Pible, O.; Degli Esposti, D.; Gaillard, J.-C.; Chaumot, A.;
911 Geffard, O.; Armengaud, J. Digging Deeper Into the Pyriproxyfen-Response of the Amphipod
912 Gammarus Fossarum With a Next-Generation Ultra-High-Field Orbitrap Analyser: New
913 Perspectives for Environmental Toxicoproteomics. *Front. Environ. Sci.* **2018**, *6*.
914 <https://doi.org/10.3389/fenvs.2018.00054>.
- 915 (57) Liu, H.; Sadygov, R. G.; Yates, J. R. A Model for Random Sampling and Estimation of Relative
916 Protein Abundance in Shotgun Proteomics. *Anal. Chem.* **2004**, *76* (14), 4193–4201.
917 <https://doi.org/10.1021/ac0498563>.

- 918 (58) Perez-Riverol, Y.; Csordas, A.; Bai, J.; Bernal-Llinares, M.; Hewapathirana, S.; Kundu, D. J.;
919 Inuganti, A.; Griss, J.; Mayer, G.; Eisenacher, M.; Pérez, E.; Uszkoreit, J.; Pfeuffer, J.;
920 Sachsenberg, T.; Yilmaz, Ş.; Tiwary, S.; Cox, J.; Audain, E.; Walzer, M.; Jarnuczak, A. F.; Ternent,
921 T.; Brazma, A.; Vizcaíno, J. A. The PRIDE Database and Related Tools and Resources in 2019:
922 Improving Support for Quantification Data. *Nucleic Acids Res.* **2019**, *47* (D1), D442–D450.
923 <https://doi.org/10.1093/nar/gky1106>.
- 924 (59) Li, H.-D.; Xu, Q.-S.; Liang, Y.-Z. LibPLS: An Integrated Library for Partial Least Squares
925 Regression and Linear Discriminant Analysis. *Chemom. Intell. Lab. Syst.* **2018**, *176*, 34–43.
926 <https://doi.org/10.1016/j.chemolab.2018.03.003>.
- 927 (60) Bylesjö, M.; Rantalainen, M.; Nicholson, J. K.; Holmes, E.; Trygg, J. K-OPLS Package: Kernel-
928 Based Orthogonal Projections to Latent Structures for Prediction and Interpretation in Feature
929 Space. *BMC Bioinformatics* **2008**, *9* (1), 106. <https://doi.org/10.1186/1471-2105-9-106>.
- 930 (61) Darzi, Y.; Letunic, I.; Bork, P.; Yamada, T. IPath3.0: Interactive Pathways Explorer V3. *Nucleic*
931 *Acids Res.* **2018**, *46* (W1), W510–W513. <https://doi.org/10.1093/nar/gky299>.
- 932 (62) Bradley, P. H.; Brauer, M. J.; Rabinowitz, J. D.; Troyanskaya, O. G. Coordinated Concentration
933 Changes of Transcripts and Metabolites in *Saccharomyces Cerevisiae*. *PLOS Comput. Biol.*
934 **2009**, *5* (1), e1000270. <https://doi.org/10.1371/journal.pcbi.1000270>.
- 935 (63) Hirai, M. Y.; Klein, M.; Fujikawa, Y.; Yano, M.; Goodenowe, D. B.; Yamazaki, Y.; Kanaya, S.;
936 Nakamura, Y.; Kitayama, M.; Suzuki, H.; Sakurai, N.; Shibata, D.; Tokuhisa, J.; Reichelt, M.;
937 Gershenzon, J.; Papenbrock, J.; Saito, K. Elucidation of Gene-to-Gene and Metabolite-to-Gene
938 Networks in Arabidopsis by Integration of Metabolomics and Transcriptomics. *J. Biol. Chem.*
939 **2005**, *280* (27), 25590–25595. <https://doi.org/10.1074/jbc.M502332200>.
- 940 (64) Hirai, M. Y.; Yano, M.; Goodenowe, D. B.; Kanaya, S.; Kimura, T.; Awazuhara, M.; Arita, M.;
941 Fujiwara, T.; Saito, K. Integration of Transcriptomics and Metabolomics for Understanding of
942 Global Responses to Nutritional Stresses in Arabidopsis Thaliana. *Proc. Natl. Acad. Sci. U. S. A.*
943 **2004**, *101* (27), 10205–10210. <https://doi.org/10.1073/pnas.0403218101>.
- 944 (65) Nikiforova, V. J.; Daub, C. O.; Hesse, H.; Willmitzer, L.; Hoefgen, R. Integrative Gene-
945 Metabolite Network with Implemented Causality Deciphers Informational Fluxes of Sulphur
946 Stress Response. *J. Exp. Bot.* **2005**, *56* (417), 1887–1896. <https://doi.org/10.1093/jxb/eri179>.
- 947 (66) Gibon, Y.; Usadel, B.; Blaesing, O. E.; Kamlage, B.; Hoehne, M.; Trethewey, R.; Stitt, M.
948 Integration of Metabolite with Transcript and Enzyme Activity Profiling during Diurnal Cycles
949 in Arabidopsis Rosettes. *Genome Biol.* **2006**, *7* (8), R76. [https://doi.org/10.1186/gb-2006-7-8-](https://doi.org/10.1186/gb-2006-7-8-r76)
950 [r76](https://doi.org/10.1186/gb-2006-7-8-r76).
- 951 (67) Carrari, F.; Baxter, C.; Usadel, B.; Urbanczyk-Wochniak, E.; Zanon, M.-I.; Nunes-Nesi, A.;
952 Nikiforova, V.; Centero, D.; Ratzka, A.; Pauly, M.; Sweetlove, L. J.; Fernie, A. R. Integrated
953 Analysis of Metabolite and Transcript Levels Reveals the Metabolic Shifts That Underlie
954 Tomato Fruit Development and Highlight Regulatory Aspects of Metabolic Network Behavior.
955 *Plant Physiol.* **2006**, *142* (4), 1380–1396. <https://doi.org/10.1104/pp.106.088534>.
- 956 (68) Urbanczyk-Wochniak, E.; Baxter, C.; Kolbe, A.; Kopka, J.; Sweetlove, L. J.; Fernie, A. R. Profiling
957 of Diurnal Patterns of Metabolite and Transcript Abundance in Potato (*Solanum Tuberosum*)
958 Leaves. *Planta* **2005**, *221* (6), 891–903. <https://doi.org/10.1007/s00425-005-1483-y>.
- 959 (69) Sarkar, S.; Rubinsztein, D. C. Inositol and IP3 Levels Regulate Autophagy—Biology and
960 Therapeutic Speculations. *Autophagy* **2006**, *2* (2), 132–134.
961 <https://doi.org/10.4161/auto.2387>.
- 962 (70) Picot, S.; Faury, N.; Arzul, I.; Chollet, B.; Renault, T.; Morga, B. Identification of the Autophagy
963 Pathway in a Mollusk Bivalve, *Crassostrea Gigas*. *Autophagy* **2020**, *16* (11), 2017–2035.
964 <https://doi.org/10.1080/15548627.2020.1713643>.
- 965 (71) Høyer-Hansen, M.; Jäättelä, M. Connecting Endoplasmic Reticulum Stress to Autophagy by
966 Unfolded Protein Response and Calcium. *Cell Death Differ.* **2007**, *14* (9), 1576–1582.
967 <https://doi.org/10.1038/sj.cdd.4402200>.
- 968 (72) Primeau, J. O.; Armanious, G. P.; Fisher, M. E.; Young, H. S. The SarcoEndoplasmic Reticulum
969 Calcium ATPase. In *Membrane Protein Complexes: Structure and Function*; Harris, J. R.,

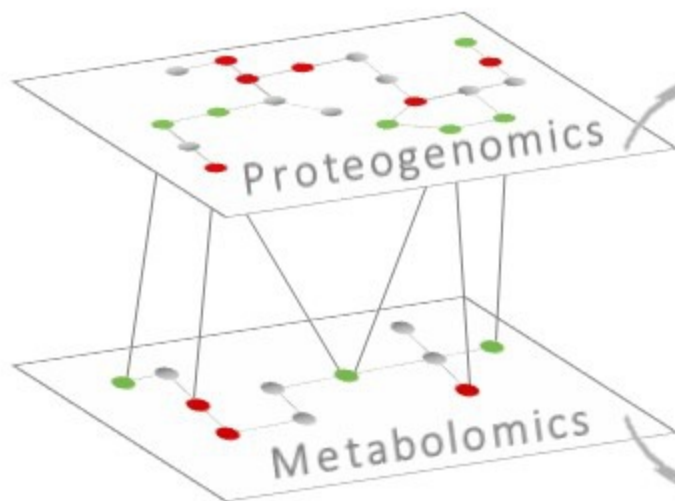
- 970 Boekema, E. J., Eds.; *Subcellular Biochemistry*; Springer: Singapore, 2018; pp 229–258.
971 https://doi.org/10.1007/978-981-10-7757-9_8.
- 972 (73) Castillo, K.; Rojas-Rivera, D.; Lisbona, F.; Caballero, B.; Nassif, M.; Court, F. A.; Schuck, S.; Ibar,
973 C.; Walter, P.; Sierralta, J.; Glavic, A.; Hetz, C. BAX Inhibitor-1 Regulates Autophagy by
974 Controlling the IRE1 α Branch of the Unfolded Protein Response. *EMBO J.* **2011**, *30* (21), 4465–
975 4478. <https://doi.org/10.1038/emboj.2011.318>.
- 976 (74) Martínez-Gómez, C.; Bignell, J.; Lowe, D. *Lysosomal Membrane Stability in Mussels*; 56;
977 International Council for the Exploration of the Sea (ICES), 2015; p 41.
978 <https://doi.org/10.25607/OBP-240>.
- 979 (75) Boya, P.; Kroemer, G. Lysosomal Membrane Permeabilization in Cell Death. *Oncogene* **2008**,
980 *27* (50), 6434–6451. <https://doi.org/10.1038/onc.2008.310>.
- 981 (76) Raftopoulou, E. K.; Dimitriadis, V. K. Aspects of the Digestive Gland Cells of the Mussel *Mytilus*
982 *Galloprovincialis*, in Relation to Lysosomal Enzymes, Lipofuscin Presence and Shell Size:
983 Contribution in the Assessment of Marine Pollution Biomarkers. *Mar. Pollut. Bull.* **2012**, *64* (2),
984 182–188. <https://doi.org/10.1016/j.marpolbul.2011.12.017>.
- 985 (77) Viarengo, A.; Lowe, D.; Bolognesi, C.; Fabbri, E.; Koehler, A. The Use of Biomarkers in
986 Biomonitoring: A 2-Tier Approach Assessing the Level of Pollutant-Induced Stress Syndrome in
987 Sentinel Organisms. *Comp. Biochem. Physiol. Toxicol. Pharmacol. CBP* **2007**, *146* (3), 281–300.
988 <https://doi.org/10.1016/j.cbpc.2007.04.011>.
- 989 (78) Schrader, M.; Costello, J.; Godinho, L. F.; Islinger, M. Peroxisome-Mitochondria Interplay and
990 Disease. *J. Inherit. Metab. Dis.* **2015**, *38* (4), 681–702. <https://doi.org/10.1007/s10545-015-9819-7>.
- 992 (79) Lawrence, A. J.; Hemingway, K. L. *Effects of Pollution on Fish: Molecular Effects and Population*
993 *Responses*; John Wiley & Sons, 2008.
- 994 (80) STANLEY-SAMUELSON, D. W. The Biological Significance of Prostaglandins and Related
995 Eicosanoids in Invertebrates. *Am. Zool.* **1994**, *34* (6), 589–598.
996 <https://doi.org/10.1093/icb/34.6.589>.
- 997 (81) Reddy, J. K.; Mannaerts, G. P. Peroxisomal Lipid Metabolism. *Annu. Rev. Nutr.* **1994**, *14* (1),
998 343–370. <https://doi.org/10.1146/annurev.nu.14.070194.002015>.
- 999 (82) Nemali, M. R.; Reddy, M. K.; Usuda, N.; Reddy, P. G.; Comeau, L. D.; Rao, M. S.; Reddy, J. K.
1000 Differential Induction and Regulation of Peroxisomal Enzymes: Predictive Value of Peroxisome
1001 Proliferation in Identifying Certain Nonmutagenic Carcinogens. *Toxicol. Appl. Pharmacol.*
1002 **1989**, *97* (1), 72–87. [https://doi.org/10.1016/0041-008X\(89\)90056-2](https://doi.org/10.1016/0041-008X(89)90056-2).
- 1003 (83) Reddy, J. K.; Lalwai, N. D. Carcinogenesis by Hepatic Peroxisome Proliferators: Evaluation of
1004 the Risk of Hypolipidemic Drugs and Industrial Plasticizers to Humans. *Crit. Rev. Toxicol.* **1983**,
1005 *12* (1), 1–58. <https://doi.org/10.3109/10408448309029317>.
- 1006 (84) Cajaraville, M. P.; Ortiz-Zarragoitia, M. Specificity of the Peroxisome Proliferation Response in
1007 Mussels Exposed to Environmental Pollutants. *Aquat. Toxicol.* **2006**, *78*, S117–S123.
1008 <https://doi.org/10.1016/j.aquatox.2006.02.016>.
- 1009 (85) Johansson, A.-C.; Appelqvist, H.; Nilsson, C.; Kågedal, K.; Roberg, K.; Öllinger, K. Regulation of
1010 Apoptosis-Associated Lysosomal Membrane Permeabilization. *Apoptosis* **2010**, *15* (5), 527–
1011 540. <https://doi.org/10.1007/s10495-009-0452-5>.
- 1012 (86) Abreu-Martin, M. T.; Chari, A.; Palladino, A. A.; Craft, N. A.; Sawyers, C. L. Mitogen-Activated
1013 Protein Kinase Kinase Kinase 1 Activates Androgen Receptor-Dependent Transcription and
1014 Apoptosis in Prostate Cancer. *Mol. Cell. Biol.* **1999**, *19* (7), 5143–5154.
1015 <https://doi.org/10.1128/MCB.19.7.5143>.
- 1016 (87) Foghsgaard, L.; Wissing, D.; Mauch, D.; Lademann, U.; Bastholm, L.; Boes, M.; Elling, F.; Leist,
1017 M.; Jäättelä, M. Cathepsin B Acts as a Dominant Execution Protease in Tumor Cell Apoptosis
1018 Induced by Tumor Necrosis Factor. *J. Cell Biol.* **2001**, *153* (5), 999–1010.
1019 <https://doi.org/10.1083/jcb.153.5.999>.

- 1020 (88) Guo, Y.; Srinivasula, S. M.; Druilhe, A.; Fernandes-Alnemri, T.; Alnemri, E. S. Caspase-2 Induces
1021 Apoptosis by Releasing Proapoptotic Proteins from Mitochondria. *J. Biol. Chem.* **2002**, *277*
1022 (16), 13430–13437. <https://doi.org/10.1074/jbc.M108029200>.
- 1023 (89) Kumar, S. Caspase 2 in Apoptosis, the DNA Damage Response and Tumour Suppression:
1024 Enigma No More? *Nat. Rev. Cancer* **2009**, *9* (12), 897–903. <https://doi.org/10.1038/nrc2745>.
- 1025 (90) Porté, S.; Valencia, E.; Yakovtseva, E. A.; Borràs, E.; Shafqat, N.; Debreczeny, J. E.; Pike, A. C.
1026 W.; Oppermann, U.; Farrés, J.; Fita, I.; Parés, X. Three-Dimensional Structure and Enzymatic
1027 Function of Proapoptotic Human P53-Inducible Quinone Oxidoreductase PIG3. *J. Biol. Chem.*
1028 **2009**, *284* (25), 17194–17205. <https://doi.org/10.1074/jbc.M109.001800>.
- 1029 (91) Romero, A.; Novoa, B.; Figueras, A. The Complexity of Apoptotic Cell Death in Mollusks: An
1030 Update. *Fish Shellfish Immunol.* **2015**, *46* (1), 79–87. <https://doi.org/10.1016/j.fsi.2015.03.038>.
- 1031 (92) Mezzelani, M.; Nardi, A.; Bernardini, I.; Milan, M.; Peruzza, L.; d’Errico, G.; Fattorini, D.; Gorbi,
1032 S.; Patarnello, T.; Regoli, F. Environmental Pharmaceuticals and Climate Change: The Case
1033 Study of Carbamazepine in *M. Galloprovincialis* under Ocean Acidification Scenario. *Environ.*
1034 *Int.* **2021**, *146*, 106269. <https://doi.org/10.1016/j.envint.2020.106269>.
- 1035 (93) Yan, S.; Chen, R.; Wang, M.; Zha, J. Carbamazepine at Environmentally Relevant
1036 Concentrations Caused DNA Damage and Apoptosis in the Liver of Chinese Rare Minnows
1037 (*Gobiocypris Rarus*) by the Ras/Raf/ERK/P53 Signaling Pathway. *Environ. Pollut.* **2021**, *270*,
1038 116245. <https://doi.org/10.1016/j.envpol.2020.116245>.
- 1039 (94) Pytharopoulou, S.; Kouvela, E. C.; Sazakli, E.; Leotsinidis, M.; Kalpaxis, D. L. Evaluation of the
1040 Global Protein Synthesis in *Mytilus Galloprovincialis* in Marine Pollution Monitoring: Seasonal
1041 Variability and Correlations with Other Biomarkers. *Aquat. Toxicol.* **2006**, *80* (1), 33–41.
1042 <https://doi.org/10.1016/j.aquatox.2006.07.010>.
- 1043 (95) Sokolova, I. M.; Frederich, M.; Bagwe, R.; Lannig, G.; Sukhotin, A. A. Energy Homeostasis as an
1044 Integrative Tool for Assessing Limits of Environmental Stress Tolerance in Aquatic
1045 Invertebrates. *Mar. Environ. Res.* **2012**, *79*, 1–15.
1046 <https://doi.org/10.1016/j.marenvres.2012.04.003>.
- 1047 (96) Almeida, Â.; Freitas, R.; Calisto, V.; Esteves, V. I.; Schneider, R. J.; Soares, A. M. V. M.; Figueira,
1048 E. Chronic Toxicity of the Antiepileptic Carbamazepine on the Clam *Ruditapes Philippinarum*.
1049 *Comp. Biochem. Physiol. Toxicol. Pharmacol. CBP* **2015**, *172–173*, 26–35.
1050 <https://doi.org/10.1016/j.cbpc.2015.04.004>.
- 1051 (97) Parolini, M.; Quinn, B.; Binelli, A.; Provini, A. Cytotoxicity Assessment of Four Pharmaceutical
1052 Compounds on the Zebra Mussel (*Dreissena Polymorpha*) Haemocytes, Gill and Digestive
1053 Gland Primary Cell Cultures. *Chemosphere* **2011**, *84* (1), 91–100.
1054 <https://doi.org/10.1016/j.chemosphere.2011.02.049>.
- 1055

Solvent
Control



Carbamazepine
80 $\mu\text{g/L}$



Mid-level data fusion

MCUVE-PLS &
consensus OPLS-DA

Metabolic & Cellular stress

- Amino acid, purine and lipid metabolisms
- Protein synthesis process
- Transport and catabolism processes

HYPOTHESES

- Autophagy induction
- Lysosomal membrane destabilization
- Peroxisomes and mitochondria dysfunction
- Apoptosis